AFSWC-TDR-62-90

SWC
TDR
62-90

LABORATORY EXPERIMENTS ON THE RESPONSE OF SOILS TO SHOCK LOADINGS

TECHNICAL DOCUMENTARY REPORT NO. AFSWC-TDR-62-90

January 1963

Research Directorate
AIR FORCE SPECIAL WEAPONS CENTER
Air Force Systems Command
Kirtland Air Force Base
New Mexico

This research has been funded by the Defense Atomic Support Agency under WEB No. 13.004

Project No. 1080, Task No. 108001

(Prepared under Contract No. AF 29(601)-2830 by G. A. Leonards, Purdue University, School of Civil Engineering, Lafayette, Indiana)

HEADQUARTERS
AIR FORCE SPECIAL WEAPONS CENTER
Air Force Systems Command
Kirtland Air Force Base
New Mexico

TDR-62-90

ABSTRACT

A report is made of research being carried out at Purdue University whose overall purpose is to develop, on the basis of direct measurements, mathematical models suitable for describing the propagation of a compression shock wave through soils--principally through partly saturated clays. This interim report deals with the selection of a suitable type of laboratory test and with the design, calibration, and use of gages to measure stress and strain in the vicinity of a point during the propagation of a shock wave. Preliminary results from tests on samples of compacted clay are also included.

PUBLICATION REVIEW

This report has been reviewed and is approved.

for Perry L. Huie Col USAF
DONALD I. PRICKETT
Colonel USAF
Director, Research Directorate

John J. Dishuck
JOHN J. DISHUCK
Colonel USAF
DCS/Plans & Operations

TABLE OF CONTENTS

LIST OF FIGURES

LIST OF TABLES

INTRODUCTION

The work reported herein was carried out under Contract No. AF 29(601)-2830, "Study and Design of a Laboratory Experiment on the Dynamic Properties of Soils," an integral part of a large-scale research program on protective construction sponsored by the United States Air Force. The objective of the present study is to determine by direct measurements the actual behavior of a clay soil through which a compressional shock wave is being propagated with a view towards establishing a realistic mathematical model to describe the soil's response.

This document constitutes an interim report covering studies completed during the period September 1, 1960 to June 30, 1962.

Criteria for a suitable type of laboratory test were first established. These included:

1. Propagation of a shock wave (rise time to peak stress less than one millisecond) through the soil with a known input and a peak pressure intensity exceeding 100 psi.
2. Direct measurement of a sufficient number of soil parameters to permit an independent check between computed and measured results.
3. Use of a minimum number of space coordinates.

Considering the objective of the experiment, there appeared to be no alternative to the application of a true shock as an input loading (as opposed to a forced vibration) since the macroscopic response of clay soils is known to be sensitive to loading rates. To permit comparisons

between computed and experimental results the input loading should be known, which suggested the application of an air shock. An initial peak pressure intensity exceeding 100 psi was selected in order to include a stress range within which potential plastic (or visco-elastic) behavior could be detected.

Considerable thought was given to the selection of the soil parameters to be measured. Various types of available stress, displacement, velocity, and acceleration gages were studied. Largely on the basis of personal preference, the following parameters were selected for study:

1. Stress-strain relation at a point as a function of time.
2. Attenuation of the intensity of the shock wave as a function of distance.
3. Velocity at which the shock wave front is propagated through the soil.

A minimum number of space coordinates was specified simply as a matter of convenience in comparing theoretical and experimental results.

The possibility of achieving the objectives stated above by modifications of conventional soil tests was studied. Direct shear (or torsional shear) tests were rejected because the propagation of a compression wave was of primary interest. Various devices for applying a uniform shock loading to the ends of a triaxial test specimen were considered. The problems involved appeared to be too formidable for a short-term solution (this problem has not yet been solved for static loadings). From a mathematical standpoint, one dimensional (confined) loading would be ideal. The state of knowledge regarding dynamic wall friction is such that this problem must itself be elucidated before appropriate one-dimensional compression devices can be developed on a laboratory scale. These considerations led to the design of a test specimen having radial symmetry

and long enough so that in the central portion of the specimen essentially confined compression conditions exist in the axial direction. A shock wave would be propagated by detonating an explosive cord placed in a small hole through the axis of the sample. To consummate the study two items of instrumentation were needed: a dynamic stress gage and a dynamic strain gage.

The remainder of this report deals with the design, fabrication and calibration of dynamic stress and strain gages. Preliminary results obtained from tests on samples of compacted clay are also included.

The study was conceived by and carried out under the direction of Professor G. A. Leonards, with the assistance of Professor M. E. Harr. The experimental work was conducted by J. R. Bell, W. Baron and J. M. Mlynarik.

STRESS GAGES

Construction

The stress gages are of the piezoelectric type similar to those constructed at the Armour Research Foundation (1)*. An exploded view of the essential elements of the gage are shown in Figure 1. The dimensions of the bakelite base and brass sleeve are shown in Figure 2. The sleeve and base are machined to provide a light press fit. The stress-sensing element is a barium titanate ceramic crystal in the form of a tube approximately 1/8 inch long, 1/8 inch diameter, and 0.02 inch wall thickness (Model PZT-5, Part No. 2-2015-5).**

Two parts A and one part B of Epoxy 220*** are mixed, a thin coat applied to the top of the base and the bottom of the sleeve, and the two pressed firmly together. The gage leads are passed through the holes in the base, a thin coat of Epoxy applied to the bottom of the crystal, and the leads pulled through (gently but firmly) to seat the crystal on the base. A 1/8 inch diameter cellulose acetate cap 0.02 inches thick is similarly bonded to the top of the crystal. While the Epoxy is still wet the gage is placed in a jig so that small weights may be suspended from the leads to keep the crystal in place, all parts are carefully centered, and the Epoxy allowed to cure for 24 hours.

---

* The References are given on page 23.

** Clevite Electronic Components Division, Clevite Corporation, Cleveland 14, Ohio

*** An Opticon product made by Hughes Associates, Excelsior, Minnesota

A mixture of 100 parts (by weight) of C-2 Adhesive, 35 parts Flexible Resin No. 1, and 11 parts of Activator A* is prepared and thoroughly mixed until the resulting potting compound acquires a milky color. The space between the crystal and the brass sleeve is filled with potting compound, care being taken to eliminate the formation of air bubbles. The compound is allowed to cure for 24 hours; any excess is carefully filed off the top of the gage.

The polarity of the gage is tested by connecting it to a D.C. voltmeter (or an oscilloscope) and the gage squeezed between the fingers. The negative lead is soldered to the shielded side of a coaxial cable and the positive lead to the center conductor. The soldered connections are painted with Epoxy 220 and after curing are wrapped with Teflon adhesive tape to waterproof the connections. A photograph of the assembled gage is shown in Figure 3. After assembly is complete, the space between the leads and the holes in the base of the gage is sealed with Epoxy.

Circuitry

When stressed, the barium titanate crystal develops a charge on its surface. The response is essentially instantaneous. The developed charge per psi of applied pressure is called the gage factor (K_f) and is about 60 $\mu\mu$ Coulombs/p.s.i. for the crystals used in this study. The charge will remain constant as long as the stress remains constant except for leakage through external paths.

In practice, the charge on the crystal is not measured directly. Instead, the developed voltage is measured when the charge is discharged through the recording circuitry. Accordingly, to measure dynamic stress changes the rate of this discharge must be small in comparison to the

*Manufactured by the Armstrong Company, Warsaw, Indiana

stress duration that is of interest. The discharge rate is controlled by the impedance of the discharge path, the higher the impedance the slower the discharge rate. The early tests reported herein utilized cathode-followers having an input impedance of 10 megohms. A minor amount of decay was encountered and later tests incorporated Columbia Research Laboratories, Series 4000 cathode-followers with an input impedance of 5000 megohms.

The output voltage was measured with a Tektronix Model 502 dual beam oscilloscope with single sweep trigger lock-out circuitry. The record was photographed with a Tektronix Oscilloscope Camera Model C-12 and Polaroid 3000 speed film. Since the voltage recorded is a function of the circuitry used, a calibration procedure is necessary to relate the developed voltage to the charge on the crystal.

Calibration

The calibration procedure used is similar in principle to that developed by Soroka and Wenig (2). The arrangement is shown schematically in Figure 4. With the switch in the calibration position, a calibration capacitor (C_c) is placed in series with the square wave calibration voltage (E_c) of the oscilloscope. The observed deflection (D_c) on the oscilloscope is

$$D_c = \frac{C_c\ E_c\ A_{cF}}{C_c + C_g + C_\ell + C_s} \quad \text{- - - - - - - - - - - - - - (1)}$$

where C_g, C_ℓ, C_s = capacitances of the gage, line, and stray

A_{cF} = amplification factor of the cathode follower

With the switch in the test position, the deflection (D_f) due to the voltage generated by the crystal subjected to an applied stress (σ) is

$$D_f = \frac{K_f \, \sigma \, A_{cF}}{C_c + C_g + C_\ell + C_s} \qquad \text{- - - - - - - - - - - - - (2)}$$

where, K_f = gage factor.

The ratio

$$\frac{D_f}{D_c} = \frac{K_f \sigma}{C_c E_c}\,, \text{ or } \sigma = \frac{D_f}{D_c}\left[\frac{C_c E_c}{K_f}\right] \qquad \text{- - - - - - - - - - (3)}$$

Thus, if the gage factor is known, the applied stress can be determined from the ratio of the oscilloscope deflections during the test and during calibration.

The gage factor can be determined from Equation 3 by applying a known pressure pulse to the gage. This can be accomplished in a variety of ways. In this study a shock tube was used because of the small rise-times that can be obtained and because the tube could be used for other purposes in a related study.

Shock Tube Relationships

If a pressure difference is applied across a diaphragm, and the diaphragm suddenly burst, a shock wave will be propagated in a direction from the high to low pressure and a rarefaction wave generated in the opposite direction. These conditions are shown schematically below with the various zones numbered for convenience in discussion.

Initial Condition

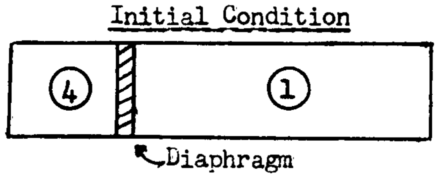

During shock wave propagation

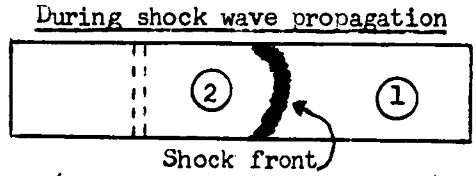

(Rarefaction wave not shown)

If the following assumptions are made:

1. Tube of constant cross-section
2. Driver gas and driven gas at same temperature
3. Flow is one dimensional, with no viscosity effect and no heat flow at the boundary
4. Thermodynamically perfect (c_v, c_p constant) ideal ($pv = RT$) gas
5. Instantaneous diaphragm burst

Then (3),

$$p_{41} = p_{21}\left[1 - \left\{p_{21} - 1\right\}\sqrt{\frac{\beta_4\, E_{14}}{\alpha_1\, p_{21} + 1}}\right]^{-1/\beta_4} \quad \ldots\ldots\ldots\ldots (4)$$

$$= \frac{1}{\alpha_1}\left\{\frac{M_s}{\beta_1} - 1\right\}\left[1 - \frac{(\gamma_4 - 1)}{(\gamma_1 + 1)\, A_{41}}\left\{\frac{M_s^2 - 1}{M_s}\right\}\right]^{-1/\beta_4} \quad \ldots (5)$$

where, p_{41} = initial pressure ratio across diaphragm (p_4/p_1, absolute press.)

p_{21} = pressure ratio across shock front (p_2/p_1, absolute press.)

c_v = specific heat at constant volume

c_p = specific heat at constant pressure

γ = c_p/c_v

α = $(\gamma + 1)/(\gamma - 1)$

β = $(\gamma - 1)/2\gamma$

E = internal energy, $c_v\, T$ (T = absolute temperature)

E_{14} = $E_1/E_4 = c_{v_1}/c_{v_4}$ (at constant temperature)

M_s = Mach number of shock front velocity (ratio of shock front velocity to the speed of sound in the driven gas 1)

a = speed of sound

$A_{41} = a_4/a_1 = \sqrt{\frac{\gamma_4\, m_1}{\gamma_1\, m_4}}$ (const. temperature)

m = molecular weight

For AIR (4) / AIR (1) (for the stated assumptions)

$$\frac{1}{p_{41}} = \frac{1}{p_{21}} \left[1 - \frac{p_{21} - 1}{\sqrt{41.35\, p_{21} + 6.944}} \right]^{6.944} \quad \ldots\ldots (6)$$

$$p_{21} = 1.167 \left\{ M_s^2 - 0.144 \right\} \quad \ldots\ldots\ldots\ldots\ldots (7)$$

Equations 6 and 7 are plotted in Figures 5 and 6, respectively.

The piezoelectric crystal responds only to the stress change $\Delta p = p_2 - p_1 = p_1 (p_{21} - 1)$ as the shock front moves across the gage. While high Mach numbers can be obtained by increasing p_{21} (Eqn. 7), large values of Δp can be achieved only if both p_{21} and p_1 are large. Thus, for a given value of p_4 there is an optimum value of p_1 which gives the largest value of Δp. The locus of points corresponding to this optimum combination is plotted in Figure 7. For example, with p_4 = 200 p.s.i. the largest value of Δp that can be obtained is 47 p.s.i. if p_1 is made equal to 56 p.s.i. (note that Δp is a pressure change, p_1 and p_4 are absolute pressures).

Shock Tube Construction

A shock tube was constructed of 3 inch O.D. stainless steel with 1/8 inch wall thickness. The high-pressure chamber is 18 inches long and the low-pressure chamber is 48 inches long. Provision was made to lengthen either or both chambers as desired. The sections are connected by bolting together 5 1/2 inch diameter flanges 3/8 inch thick, which are welded to the tube. O-ring seals are used between the flanges. Gage mounts 12 inches on center are located in the low-pressure chamber to securely hold the gages in place. A detail of the gage mount is shown in Figure 8. A manual trigger was designed (Fig. 9) which provides

an effective seal, bursts the diaphragm cleanly, and is simple to construct.

Mylar polyester was first used as a diaphragm, but even when punctured at almost the maximum pressure difference it could stand, rupture occurred as a single tear. Cellulose acetate diaphragms 0.010, 0.015 and 0.020 inches thick, used singly or in combination, shatter cleanly into approximately 1/4 inch pieces and leave almost a perfect circular hole. The pressure difference these diaphragms can withstand varies with temperature and humidity; a 0.010 inch diaphragm will usually withstand 50 to 80 psi.

Figure 10 shows the shock tube with the chambers separated ready for diaphragm placement. Figure 11 is a general view of the apparatus during gage calibration. The first mount contains the gage which triggers the oscilloscope. Gages are placed in each of the other two mounts. This arrangement not only permits calibration of two gages simultaneously, but the velocity of the shock front can also be measured.

The shock tube and all appurtenances (except the recording circuitry) was constructed for about $800.

Determination of Gage Factor

From the known pressure ratio across the diaphragm the pressure ratio across the shock front (and hence Δp) is obtained from Figure 5; Δp is also obtained from the measured Mach number of the shock front (Fig. 6). If the two values of Δp agree within the precision of the measured Mach number (1 to 2 per cent of p_1) on two successive trials, the value of Δp is assumed to be known. A typical oscilloscope record is reproduced in Figure 12. For this record (upper trace),

$$\sigma = \Delta p \text{ from } p_{41} = 24.8 \text{ psi}$$

$$\sigma = \Delta p \text{ from } M_s = 25.5 \text{ psi}$$

$$D_f/D_c = 0.2045$$

$$E_c = 10.0 \text{ volts}$$

$$C_c = 816 \ \mu\mu \text{ Farads}$$

$$K_f = \frac{D_f}{D_c} \left[\frac{C_c \ E_c}{\sigma}\right] = 67.4 \ \mu\mu \text{ Coulombs/p.s.i.}$$

The gage factor is determined at several values of Δp (Fig. 13) and the average value of K_f thus determined is used in subsequent tests. Periodically, gages are re-calibrated at a selected overpressure of the order of the pressures to be measured in the soil tests.

STRAIN GAGES

Design of the dynamic strain gage was guided by the following considerations:

1. Response to free-field motions of the soil.
2. Gage length as small as possible.
3. Rugged construction.
4. Simple recording circuitry.

Construction

A schematic diagram of the strain gage developed for this study is shown in Fig. 14. In order that the gage respond to free-field motions, flanges were placed at the top and bottom in a manner similar to those used on the "spool" gage developed by United Electrodynamics (4). All sliding surfaces were carefully machined, with the shaft of the plunger protected from the soil by a plastic foam shield.

The gage acts essentially as a potentiometer. A schematic diagram of the circuit used is shown in Fig. 15. The resistance element is a Markite precision conductive plastic molded resistor*, 0.075 inches wide, 0.062 inches thick, and 0.280 inches long, with one face having a resistance of 25-30 kilohms and the opposite face a resistance less than 100 ohms. Silver wipers give low friction, low noise contacts. The voltage source across the resistance element is a D. C. power supply having a range of 0-13 volts. The voltage normally used is 10-12 volts. Using the gage as a potentiometer requires three leads instead of two,

---

* Manufactured by Markite Products Corporation, 155 Waverly Place, New York 14, New York

were the gage used as a voltage divider with an external resistance. However, the advantages of maintaining the load on the voltage source constant and the low noise achieved by keeping the current flow across the contacts extremely small outweighs the disadvantage of an additional lead. Contact current is reduced further by inserting a cathode follower between the gage and the recording oscilloscope.

Details of all the parts used in constructing the gage, as well as procedures for assembly, are given in Appendix I. A photograph of the assembled gage is shown in Figure 16.

Calibration

The gage is first calibrated statically (Fig. 17a). The lower flange is clamped to the base of the calibration device and the plunger extended until the top flange contacts the micrometer. A D. C. voltage is applied to the gage and the output measured with a vacuum tube voltmeter. The micrometer head is then turned down in increments and the output voltage recorded. Typical results are plotted in Figure 18. A linear relationship may be assumed.

To check the dynamic response of the gage, the top flange is depressed against a lever arm connected to a spring (Fig. 17b). The force required to depress the spring is approximately 10 pounds. The micrometer is turned down to contact the gage and then backed off a known distance. When the top flange is released the spring drives the upper flange upwards until contact is made with the micrometer head. Upon release of the top flange, electrical contact between the gage housing and the calibrator is broken, thereby triggering the scope (recording circuitry for the strain gage is identical to that of the stress gage). The total displacement is indicated on the micrometer.

A typical record is shown in Figure 19. For the small displacement involved, the acceleration produced by the spring would be constant (if friction in the gage is neglected), and if the voltage output is linear with displacement, the output voltage versus time curve should be parabolic. Since a parabola fits the record in Fig. 19 almost exactly, the dynamic response of the strain gage was assumed to be linear.

When embedded in soil, the gage length L_g (distance between flanges) is obtained by measuring the resistance across the output (Fig. 15) with an ohmmeter. However, the corresponding deflection of the oscilloscope for a given displacement between flanges may differ from that obtained during calibration due to variations in the voltage source and in the characteristics of the cathode followers and oscilloscopes. Accordingly, for each soil test a calibration voltage (E_c) is applied to the input of the cathode follower and the deflection (D_c) of the oscilloscope obtained. The voltage source applied across the resistance element (E_s) is measured. Then the displacement (δ) between the flanges of the strain gage from the rest position is

$$\delta = K_\delta \left[\frac{E_c \; D_\delta}{E_s \; D_c}\right] \quad \ldots\ldots\ldots\ldots\ldots\ldots \quad (8)$$

where, K_δ = strain gage factor = $\frac{1}{\text{slope}}$ of calibration curve (Figure 18)

D_δ = oscilloscope deflection due to change in output voltage caused by displacement δ

The average strain, $\varepsilon = \delta/L_g$, is then known.

DYNAMIC STRESS-STRAIN MEASUREMENTS

A series of preliminary tests were conducted to evaluate the performance of the dynamic stress and strain gages when embedded in a compacted clay. The index properties of this clay are given in Table 1. In these preliminary tests no attempt was made to achieve axial symmetry.

TABLE 1
INDEX PROPERTIES OF CROSBY "B" SOIL

Liquid limit	33
Plastic limit	20
Specific gravity solids	2.70
Clay fraction, percent	20
Proctor optimum dry unit weight, p.c.f.	107
Proctor optimum moisture content, percent	19

Cylindrical samples 10 inches in diameter and 3-1/2 inches high were compacted statically in a steel mold using procedures previously developed (5) to obtain uniform density and moisture conditions. In the majority of tests the state of compaction achieved was:

Dry unit weight	= 105 p.c.f.
Water content	= 18.5 percent
Degree of saturation	= 82 percent

Soil was placed in the mold in four layers, each layer being lightly hand tamped. Gages were placed atop the second layer (along a diameter at mid-height of sample and 2-1/2 inches radially from the center of the sample), lightly pressed horizontal with the aid of a hand level,

and loose soil hand compacted around each gage before the next layer was placed. While it is desirable that the gage leads be separate for a length long enough for the gage and coaxial cable to act independently before being connected to the coaxial cable (Figure 3), as suggested earlier by Walsh (6), it is essential that the leads be shielded at the point where they are taken out of the steel mold. During static compaction the strain gage was monitored with an ohmmeter in order to detect any relative displacements between the flanges but no measureable change was noted. A number of other compaction procedures were tried but separation took place along the compaction planes during the shock loading.

Test Procedure

A 1/2 inch diameter hole is drilled through the axis of the test cylinder (Figure 20), and the sample placed inside a reinforced concrete blast chamber. A 3-1/2 inch length of 20 grain per foot Low Energy Detonating Cord (LEDC)* is inserted and held in the center of the hole with small wire hooks. The 20 grain LEDC is connected to a DuPont "SSS" Seismograph Electric Blasting Cap by a five foot length of 1 grain per foot detonating cord (Figure 21). The blasting cap, trigger circuit, and grounding leads are taken out of the blast chamber through a small port in the wall; the coaxial cables leading from the stress and strain gages are taken out through a separate port (Figure 22). The thin metal plate on the face of the sample protects it from damage due to detonation of the blasting cap and fuse.

A block diagram of the test arrangement is shown in Figure 23. The blasting cap leads are connected to a capacitor-discharge blaster.** A wire loop is placed around the blasting cap and connected to the time-mark and trigger generator circuit (Figure 24). When the wire loop is

---

*Ensign-Bickford Corporation, Simsbury, Conn.
**Southwestern Industrial Electronics Co., Houston, Tex., (less the phone line circuit).

broken by the blast it triggers a mono-stable multivibrator (m.v.) in the trigger circuit whose output triggers the sweep on the oscilloscope. The output from this m.v. also triggers a bi-stable m.v. in the time-mark circuit which acts as a lock-out circuit for the first m.v. and triggers a second mono-stable m.v. that generates a delay pulse with a desired time interval. The output from the second mono-stable m.v. is differentiated to give a sharp outward pulse, which is applied to the "B" input of both traces on the scope to provide a common time mark that serves as a base for comparative time measurements. The stress gage is connected to its cathode follower and calibration circuit and the strain gage to its D.C. voltage source and cathode follower. The outputs from the cathode followers are connected to the "A" inputs of the oscilloscope traces. All instruments have a common ground potential. The shields of all coaxial cables and the steel sample container are connected to this ground. The polarity of the hook-ups are such that compression is positive for both stress and strain measurements.

Test Results

In the development of the gages and test procedures previously described many difficulties were encountered. Some of these were instructive, and will be described briefly.

Figure 25 shows a record obtained on a stress gage in one of the early tests. It indicates a tensile stress of about 120 psi simultaneous with the detonation of the blasting cap (i.e. an infinite stress wave propagation velocity), followed by a large pressure pulse (greater than 300 psi) going completely off scale for the remainder of the record. In this test the blasting cap was connected directly to the 20 grain IEDC, the gage leads were taken through the walls of the

steel sample container before being connected to the coaxial cable leading to the cathode follower, and the sample container was not grounded. Figure 26 is a record of a repeat test on the same sample except that the IEDC was fused (with 5 feet of one grain cord). Both these tests are illustrative of how spurious the records can be when shielding is incomplete.

Figure 27 shows a stress gage record indicating a tensile stress of about 45 psi following a pressure pulse of 90 psi. The rise-time to peak pressure is about 0.35 milliseconds, as opposed to about 0.1 to 0.2 milliseconds normally observed. Note also the rapid decay of the calibration pulse. The charge on the crystal is being dissipated during compression, due to moisture decreasing the impedance of stray paths at the lead connections. When the stress is relieved, the crystal rebounds sufficiently to indicate an apparent tension. The fact that the observed decay is due to leakage through stray paths and not through the recording circuitry is illustrated by Figure 28. The decay with the gage and leads connected is large; that through the recording circuitry is negligible. Accordingly, the importance of positively sealing all gage connections cannot be over-emphasized.

Figure 29 shows a stress record obtained when all details of gage assembly and test procedure previously described are scrupulously observed. This type of record has been duplicated many times and is believed to be a reliable stress measurement for the stated test conditions.

Figure 30 shows the first simultaneous stress-strain record obtained. The spurious strain record is due to faulty gage construction, which has since been corrected. The stress record is similar to that of Figure 29 except that the time scale was increased and the compacted clay sample had a higher degree of saturation.

Figure 31 shows a typical stress-strain record. Unfortunately, the oscilloscope setting drove part of the stress record in the first shot off scale. This was corrected in a repeat test on the same sample, and the time base was extended to obtain a complete record. The first shot increases the diameter of the hole from 1/2 to about 1-1/4 inches and partly damages the sample faces (Figure 32). The larger hole reduces the intensity of the shock wave imparted to the soil when the IEDC is detonated, resulting in a lower peak stress being transmitted through the clay. The strain gage record in the second shot indicates a tendency towards almost complete recovery of strain (the stress wave follows an earlier stress wave of much higher intensity).

Figure 33 shows the results of a more recent test wherein the same scales were used for both the first and second shots. The calibration pulses for the stress and strain gages are presented in Figure 34. The decay on the stress gage is minor; that on the strain gage is negligible.

Discussion of Results

The strain gage records (Figures 31 and 33) show the displacement between the gage flanges as the stress wave propagates through the soil. Division by the gage length (approximately 2/3 inches) gives the average strain across the gage as a function of time. In one test, stress gages were placed at radial distances of 1/2 and 4-1/2 inches from the axis of the cylindrical soil sample for the purpose of obtaining preliminary data on a) the intensity of the input shock; b) the attenuation of peak stress with radial distance; and c) the rate of propagation of the stress wave through the clay. Unfortunately, the near stress gage was severely damaged and the only record obtained was the arrival time of the shock. However, the velocity of stress wave propagation could be obtained and was found to be around 1100-1200 ft/sec. Thus the stress

wave traverses the full length of the strain gage in less than 0.05 milliseconds (ms). Since the rise time to peak stress generally ranges between 0.15 and 0.25 ms, the stress distribution along the strain gage length varies with time. This is illustrated in Figure 35 (the near flange of the strain gage and the near face of the stress gage are at the same radial distance and zero time is taken when the stress gage first senses the shock) using the data in Figure 33a. From Figure 35 the average stress across the strain gage can be obtained, which is shown plotted vs. time in Figure 36. For comparison purposes, the stress vs. time curve at the near face of the stress gage and the average strain vs. time curve are also plotted in Figure 36. It is evident that the average stress-average strain-time relationships obtained from the oscilloscope records are a good approximation to the relationships extant at a point in the soil mass, and that the development of peak strain significantly lags the peak stress when a shock wave propagates through a partly saturated clay. The time lag in the development of dynamic strains is also apparent from the results of dynamic load tests of footings on granular soil reported by Cunny and Sloan (7).

From the data shown in Figure 36, the stress vs. strain relation at a point was plotted (Figure 37). Also shown on this figure is the stress-strain relation for a second shot on the same sample. The slope of the (increasing) stress-strain curve is termed the "Apparent Dynamic Modulus" (ADM). Due to the smaller rise-time to peak stress and the greater delay in the development of peak strain in the first shot, its ADM is greater than that of the second shot - - even though the clay is densified somewhat by the first shot. Although the wave velocity was not measured in this test, its value is around 1200 feet/sec. Thus, the

ADM cannot be considered a soil property as its value can vary within wide limits depending on the shape of the stress wave being propagated.

Current Investigations. Before commencing tests to measure the stress-strain-time relation as a function of distance (in which radial symmetry will be approximated more closely), it is necessary to establish the precision with which the gage response at a given radius (r) will vary with angular position (θ). The test set-up first used for this purpose is shown in Figure 38. The results obtained are summarized in Table 2. Two factors are seen to influence the test results: a) the intensity of the shock wave is a function of θ, and b) at any given θ the details of placing soil around a given gage influences the gage response. The non-uniformity of the shock wave produces a stress variation of about 20 percent in peak stress, while packing details produce a variation of 5-10 percent in peak stress. While the rate of peak stress attenuation as a function of radial distance is not yet known, it appears desirable to attempt to reduce the non-uniformity of the stress wave and to develop improved procedures for packing soil around gages before proceeding with the larger scale tests. This work is now underway.

Table 2
RESULTS OF REPRODUCIBILITY TESTS

Gage No.	Gage Factor K_f or K_δ	Max. Defl. D_f or D_δ	Peak Stress psi	Peak Strain Percent	Time to First Impulse ms	Rise Time Peak σ or ε ms	Residual Strain-% from Static Voltage Output
First Shot							
	μμC/psi						
σ 13	72.5	2.88	164		0.24	0.18	
			(158)				
σ 5	70.0	2.65	153		0.24	0.18	
σ 12	70.0	3.40	183		0.24	0.18	
			(190)				
σ 8	63.5	3.00	200		0.24	0.18	
	inches						
ε 3-3	0.250	1.10		2.37	0.34	0.82	0.46
ε 3-4	0.254	1.70		3.42	0.31	0.79	1.48
Second Shot							
σ 13	72.5	2.68	76		0.40	.23	
			(72)				
σ 5	70.0	2.34	68		0.38	.21	
σ 12	70.0	3.30	89		0.38	.25	
			(90)				
σ 8	63.5	2.71	91		0.25	.35	
ε 3-3	0.250	1.85		1.65	0.45	0.35	0.27 [0.08]*
ε 3-4	0.254	2.35		1.92	0.35	0.40	0.37 [0.23]*

*** Brackets show residual strain scaled from oscilloscope record.**

REFERENCES

1. Durelli, A. J. and W. F. Riley (1959). "Research Studies of Stress Waves in Earth and Model Earth Media," Armour Research Foundation, AFSWC TR 60-4.

2. Soroka, B. and J. Wenig (1958). "A Precision Charge Calibration Circuit for Piezo-Gage Recording," Technical Note No. 1229, Ballistic Research Laboratories, Aberdeen Proving Ground, Maryland.

3. Glass, I. I. and J. G. Hall (1959). Handbook of Supersonic Aerodynamics, Section 18 - Shock Tubes. Navord Report 1488 (Vol. 6). Superintendent of Documents, U. S. Government Printing Office, Washington 25, D. C.

4. Winston, T. (1960). "Research Studies on Free-Field Instrumentation," United Electrodynamics Inc. AFSWC TR 60-55.

5. Leonards, G. A. (1955). "Strength Characteristics of Compacted Clays," Transactions, American Society of Civil Engineers, Vol. 120, p. 1420.

6. Walsh, H.R.J. (1960). "An Experiment on Soils Loaded Dynamically in the Shock Tube," AFSWC-TN-60-39.

7. Cunny, R. W. and R. C. Sloan (1962). Discussion on "Static and Dynamic Behavior of Small Footings" by E. T. Selig and K. E. McKee, Journal of the Soil Mechanics and Foundations Division, ASCE, Vol. 88, No. SM4 (Part 1), Fig. 29, p. 203.

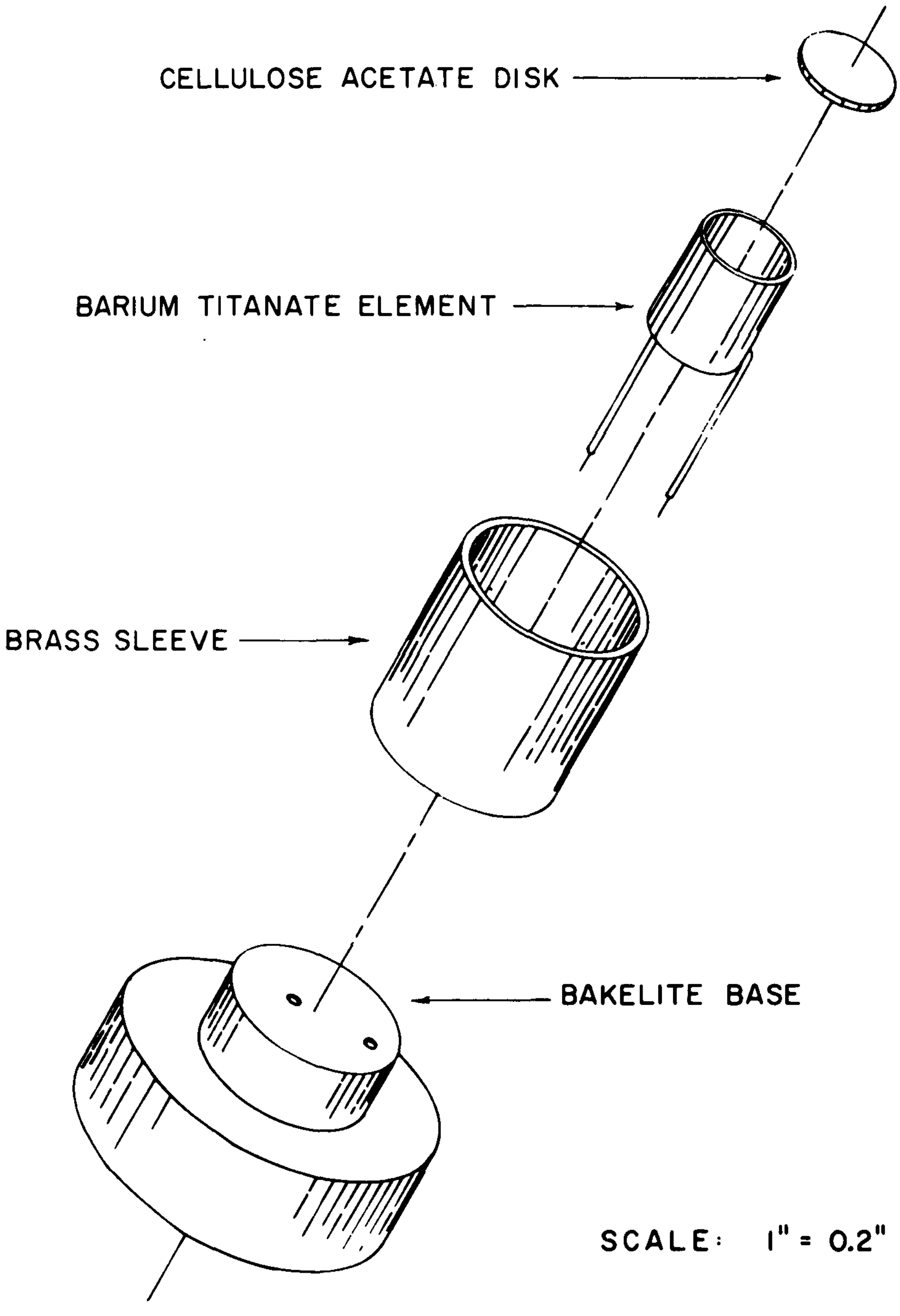

FIGURE 1. EXPLODED VIEW OF ESSENTIAL ELEMENTS OF STRESS GAGE.

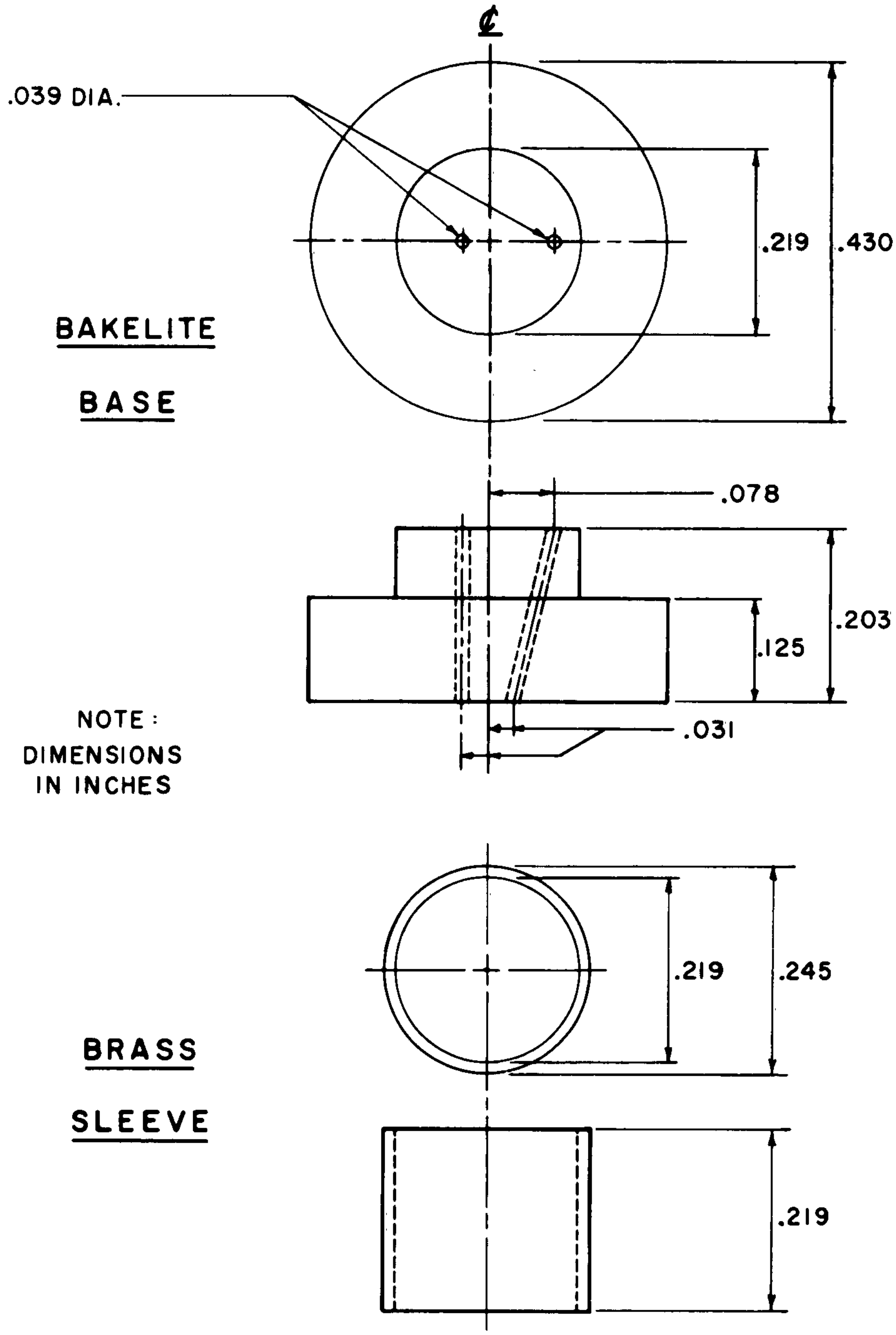

FIGURE 2. DETAILS OF BAKELITE BASE AND BRASS SLEEVE.

FIGURE 3. PHOTO OF STRESS GAGE.

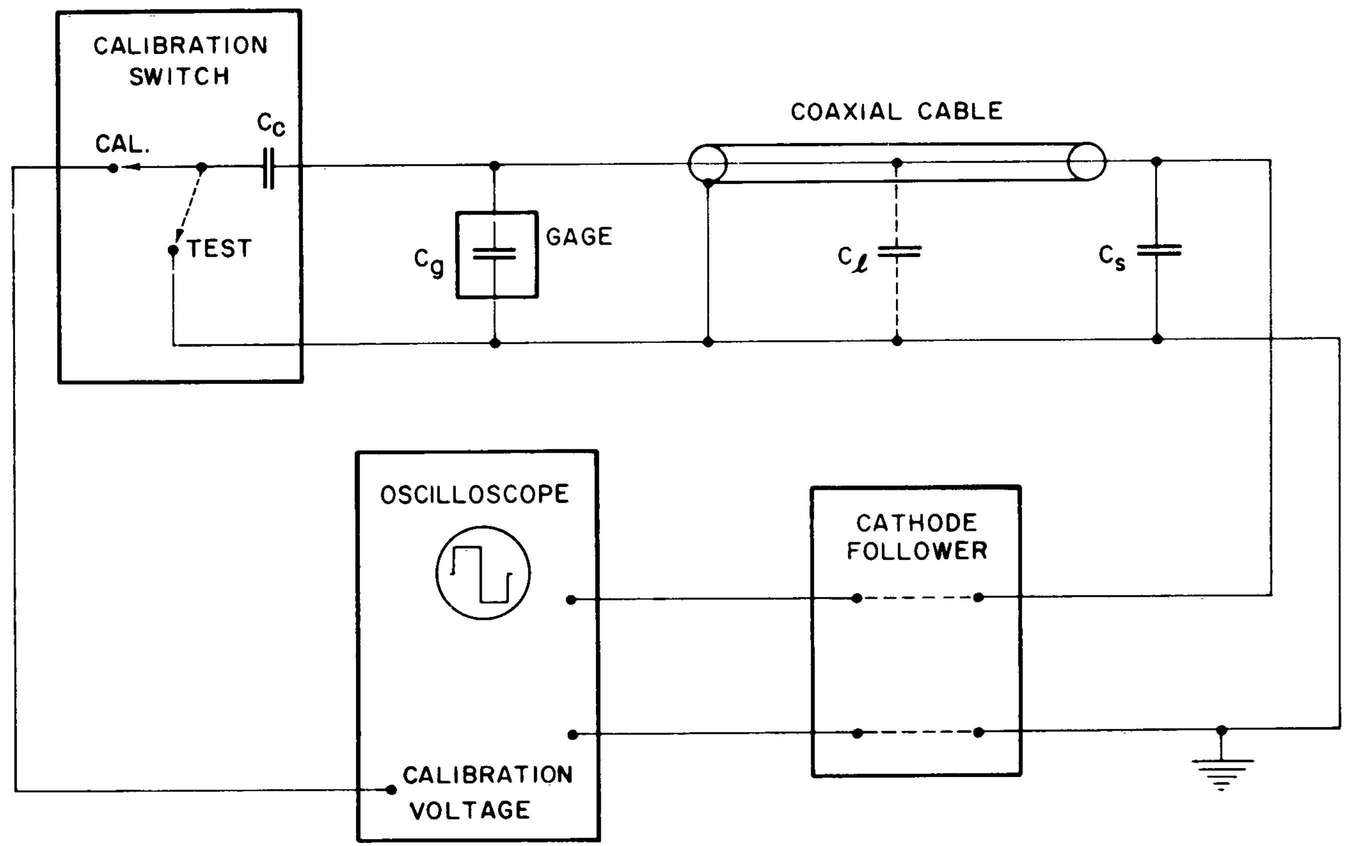

FIGURE 4. DIAGRAM OF CALIBRATION CIRCUIT.

FIGURE 5
INITIAL PRESSURE RATIO ACROSS DIAPHRAGM vs. PRESSURE RATIO ACROSS SHOCK FRONT — AIR/AIR

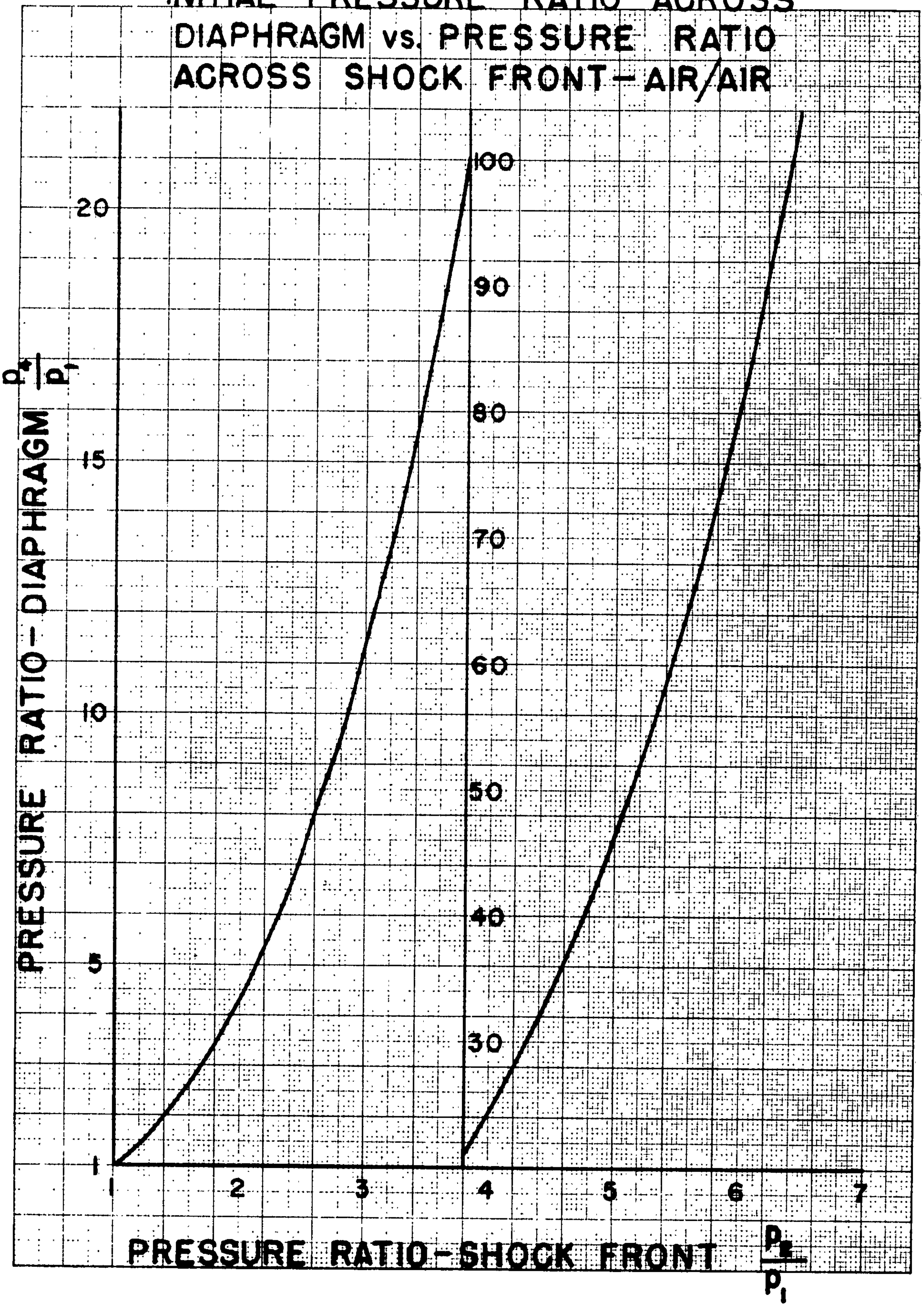

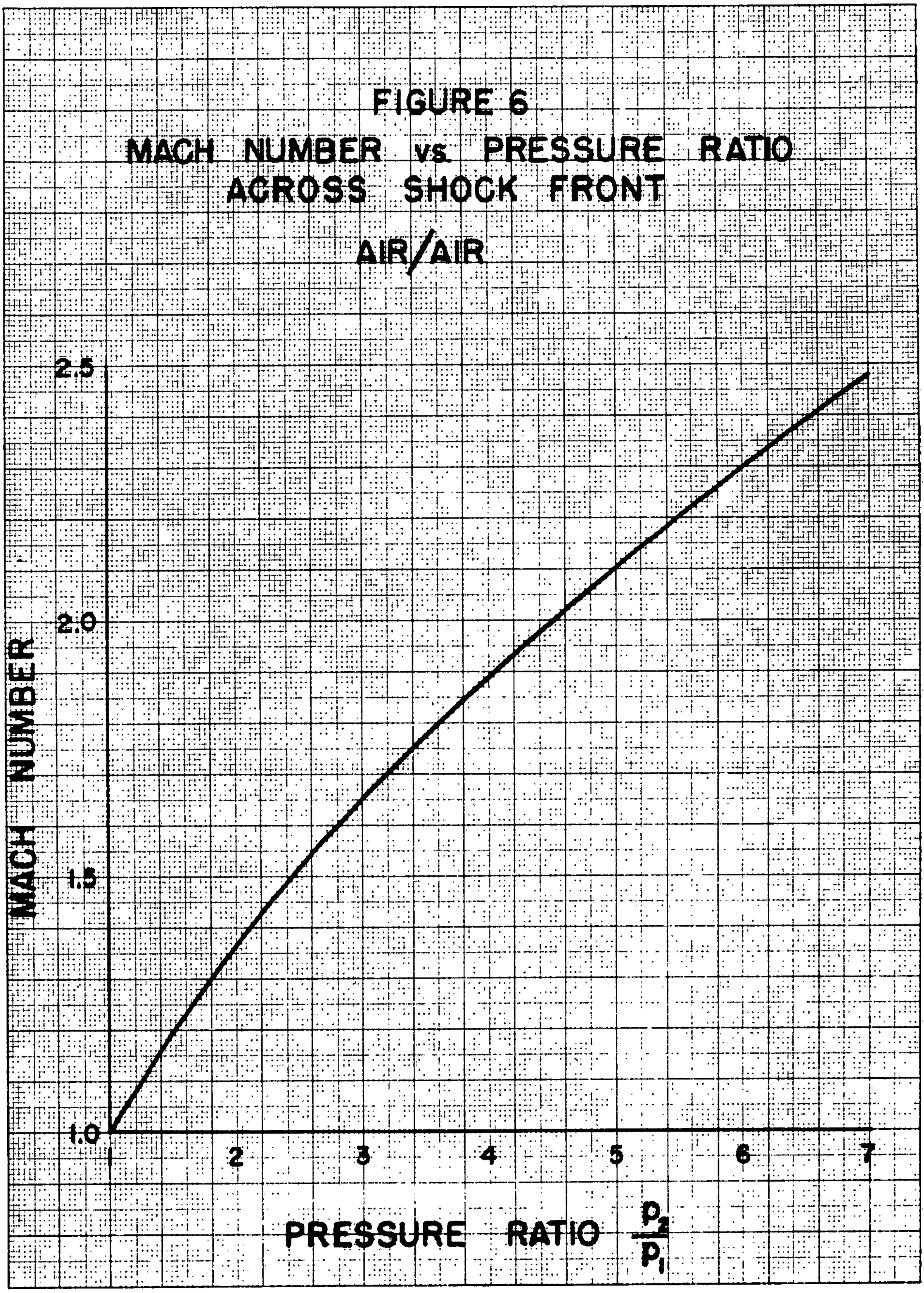
FIGURE 6
MACH NUMBER vs. PRESSURE RATIO
ACROSS SHOCK FRONT
AIR/AIR
MACH NUMBER
2.5
2.0
1.5
1.0
1
2
3
4
5
6
7
PRESSURE RATIO $\frac{p_2}{p_1}$

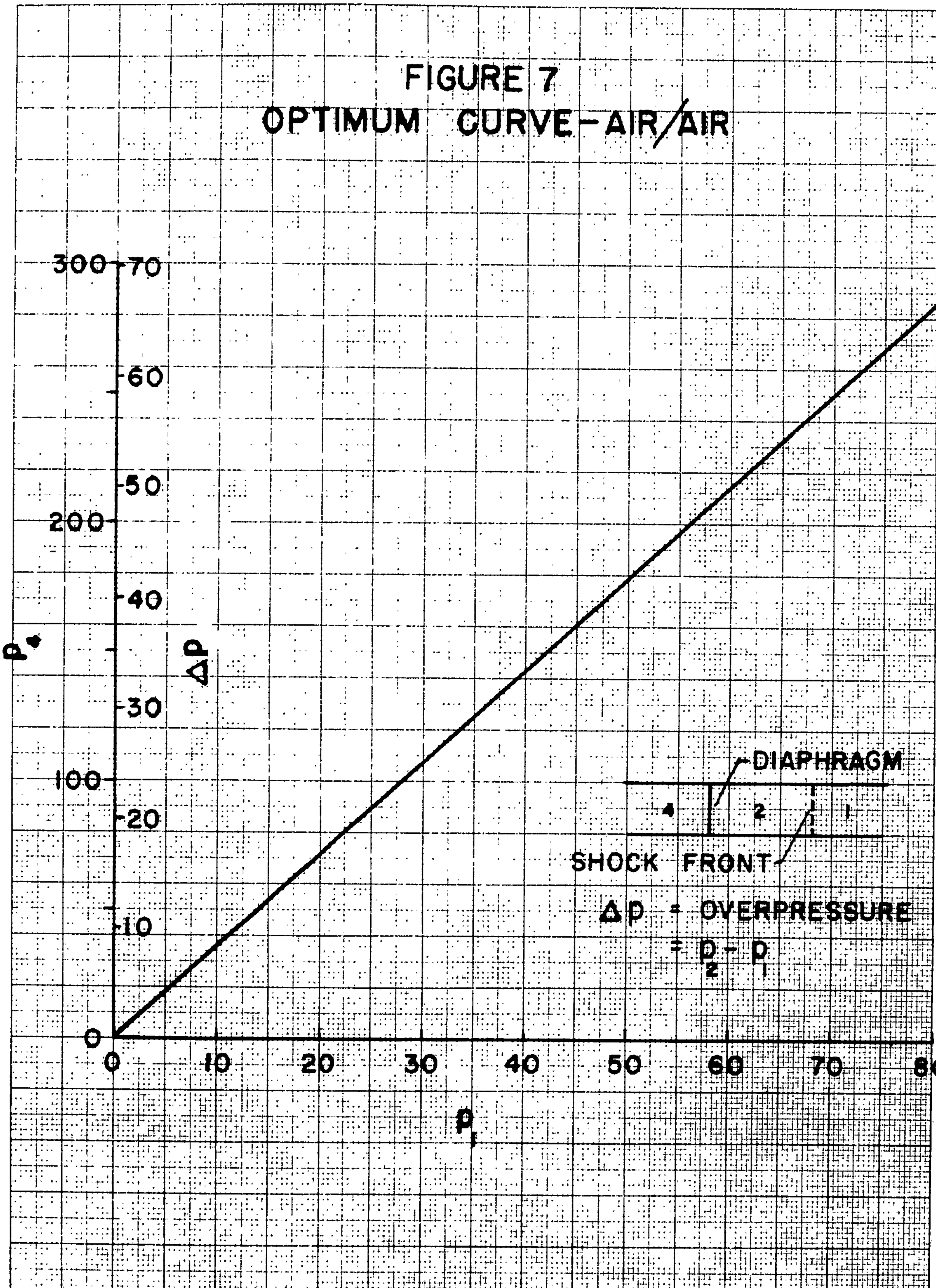
FIGURE 7
OPTIMUM CURVE-AIR/AIR
300
200
100
0
70
60
50
40
30
20
10
p_4
Δp
0
10
20
30
40
50
60
70
80
p_1
DIAPHRAGM
4
2
1
SHOCK FRONT
Δp = OVERPRESSURE
$= p_2 - p_1$

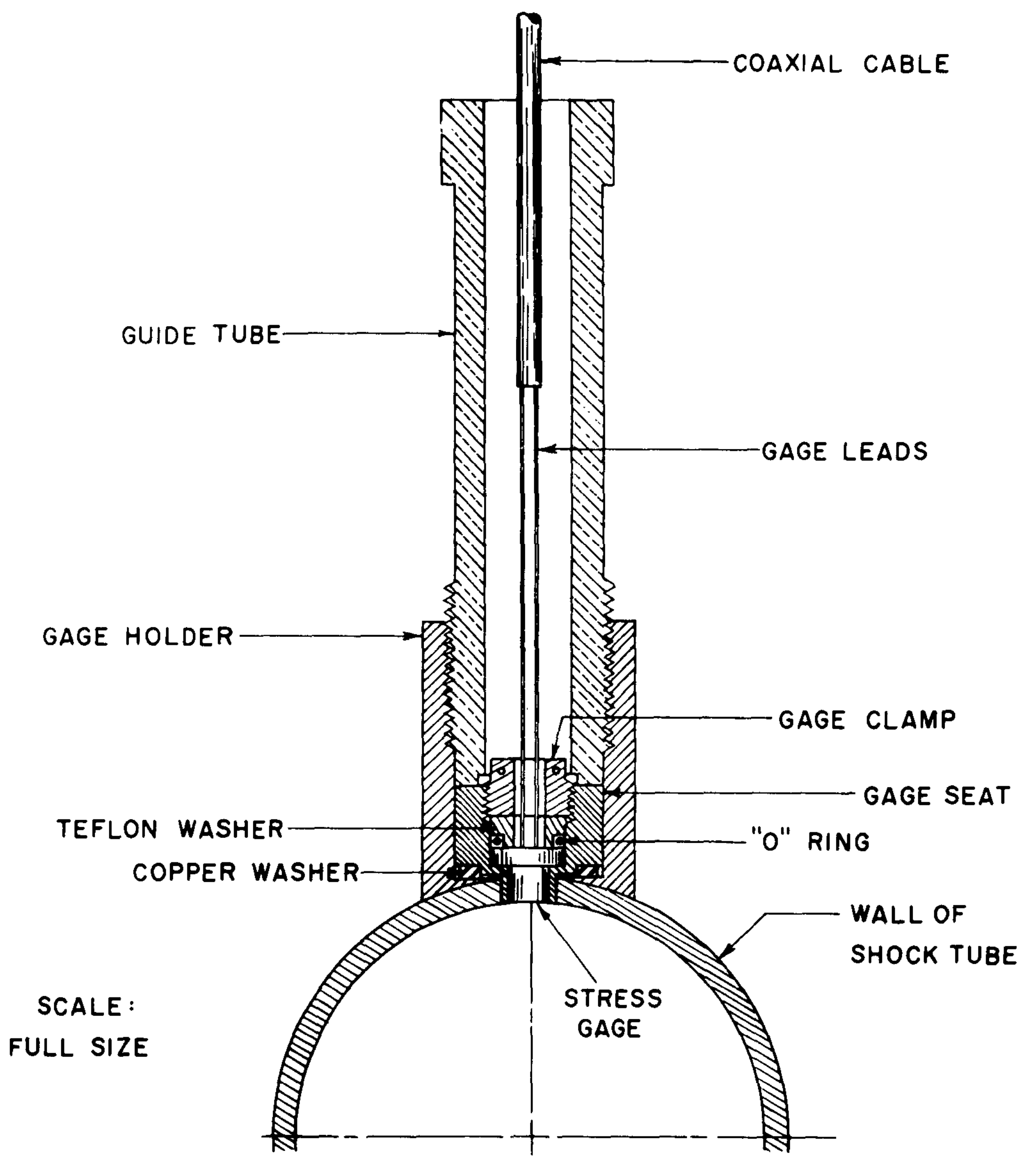

FIGURE 8. DETAIL OF GAGE MOUNT.

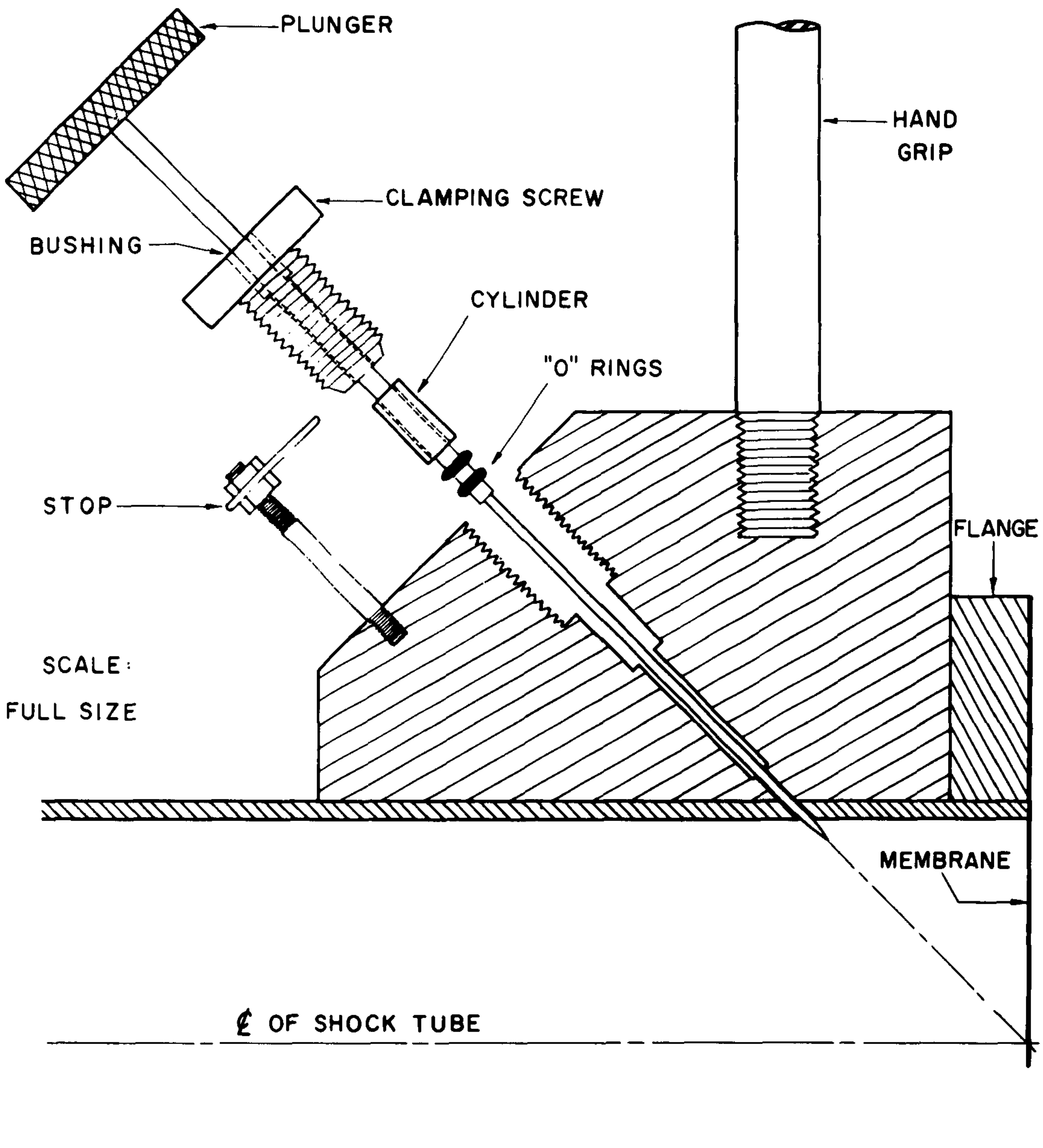

FIGURE 9. DETAIL OF MANUAL TRIGGER.

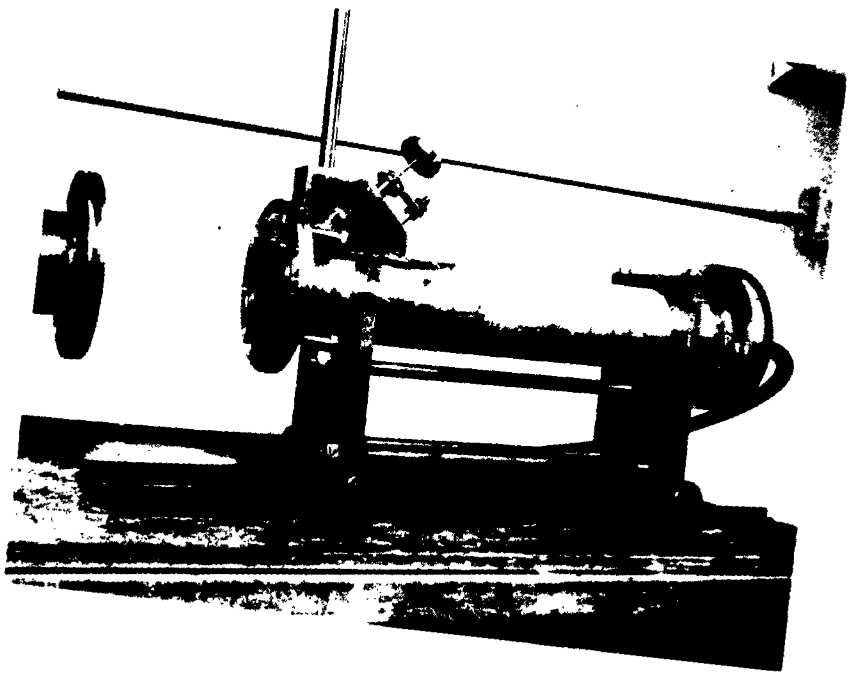

FIGURE 10. HIGH PRESSURE END OF SHOCK TUBE SHOWING MANUAL TRIGGER AND FLANGE CONNECTION OPEN FOR MEMBRANE INSERTION.

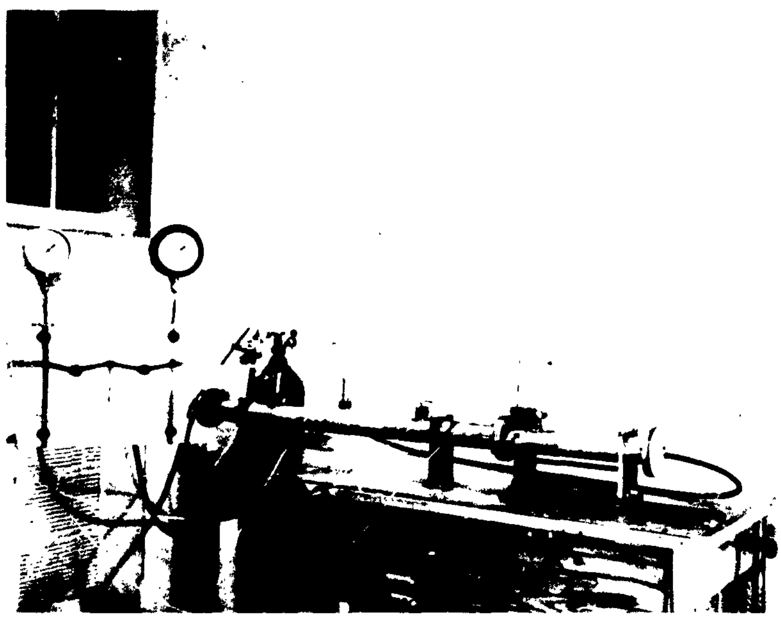

FIGURE 11. SHOCK TUBE SET-UP READY FOR GAGE CALIBRATION RUN.

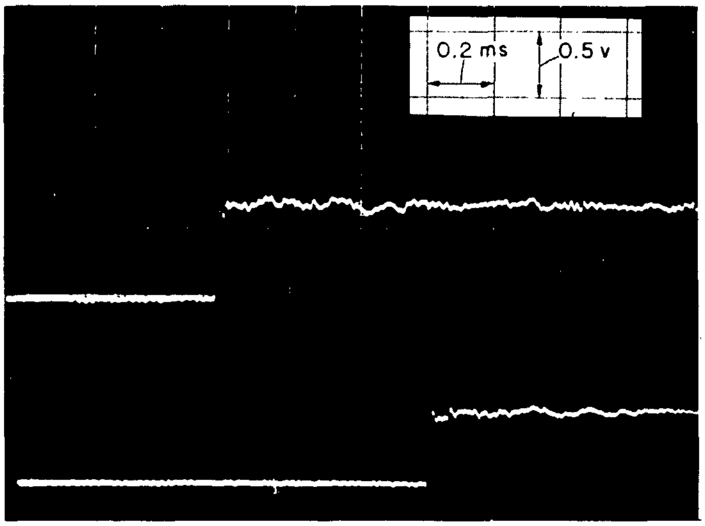

(a) Output From Stress Gage.

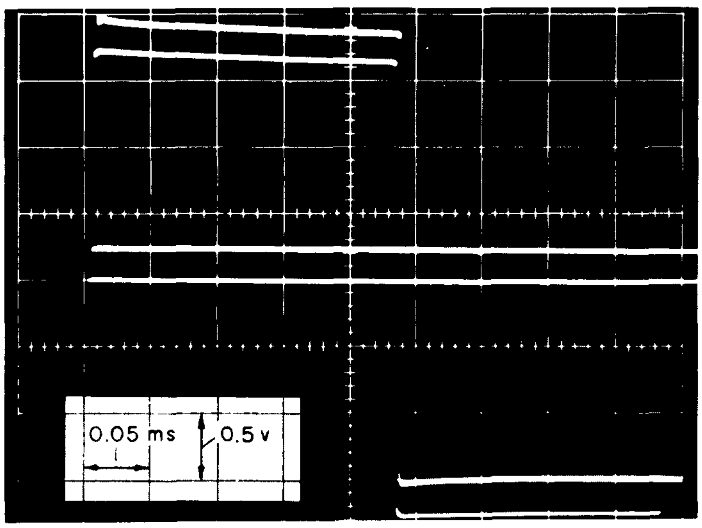

(b) Calibration Pulses.

FIGURE 12. TYPICAL RECORD OF GAGE CALIBRATION.

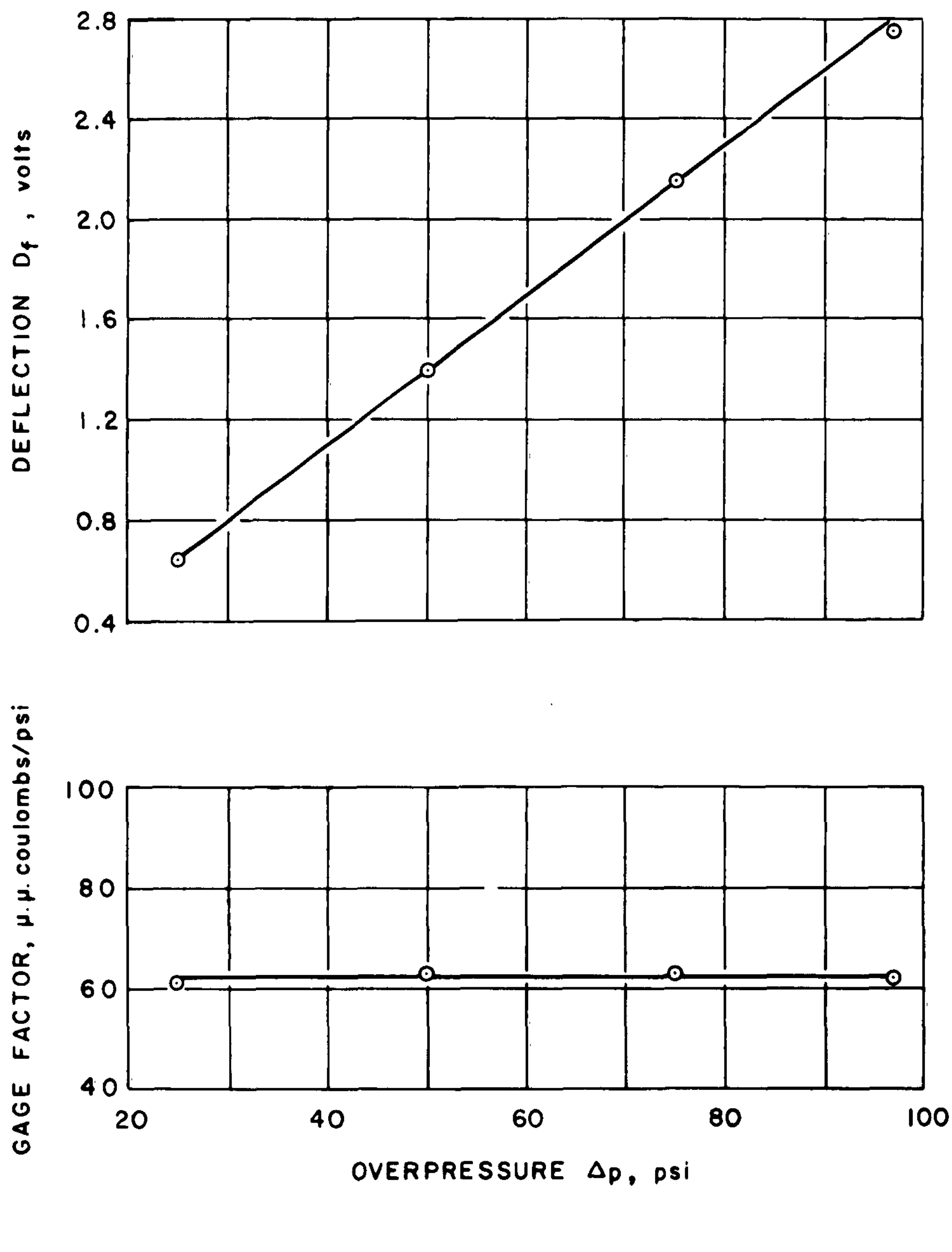

FIGURE 13. GAGE FACTOR Vs. OVERPRESSURE

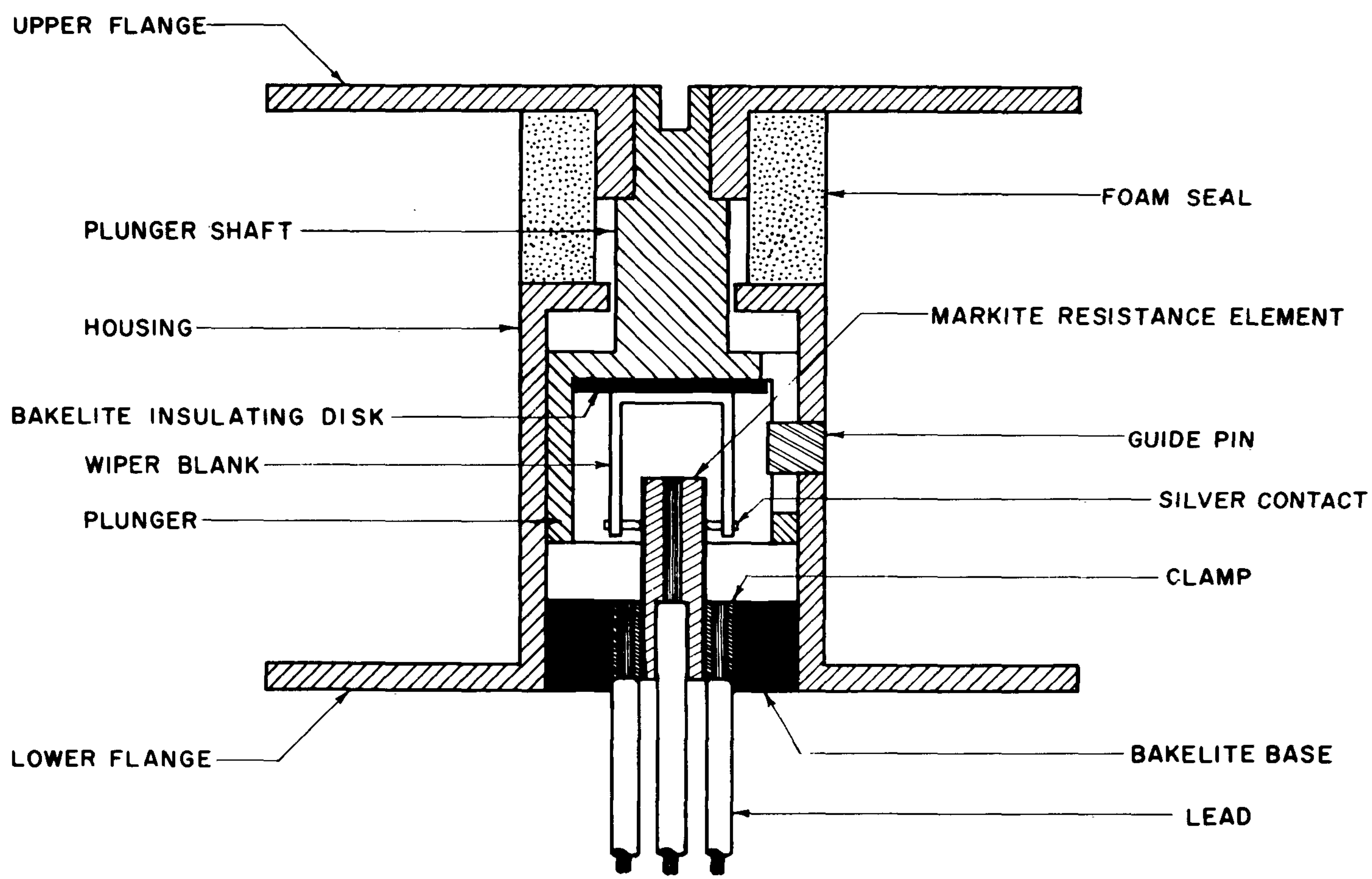

FIGURE 14. SCHEMATIC DIAGRAM OF STRAIN GAGE.

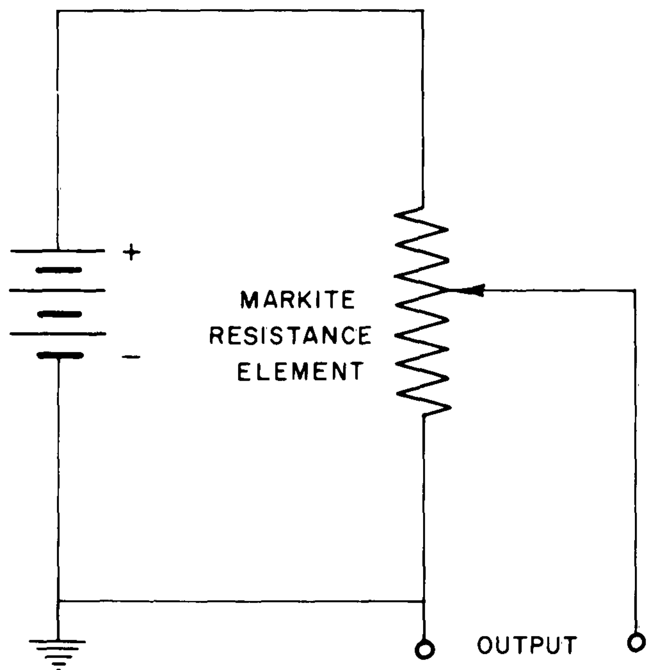

FIGURE 15. SCHEMATIC DIAGRAM OF STRAIN GAGE CIRCUIT.

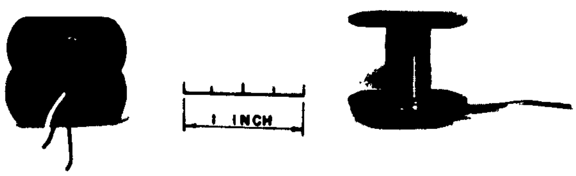

FIGURE 16. PHOTO OF ASSEMBLED STRAIN GAGE.

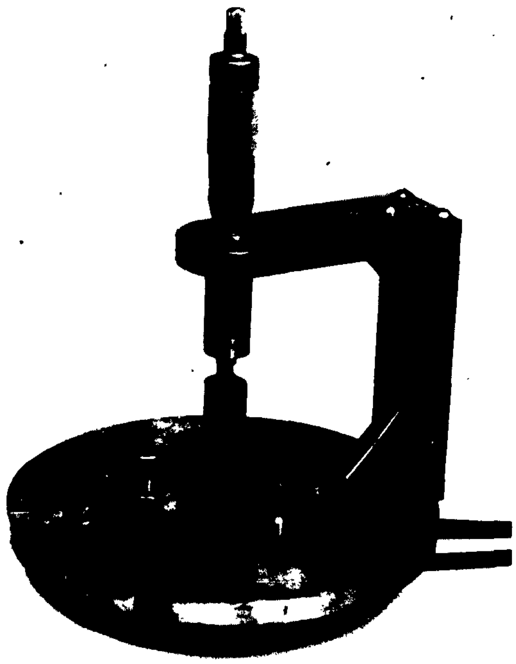

(a) Static Calibration.

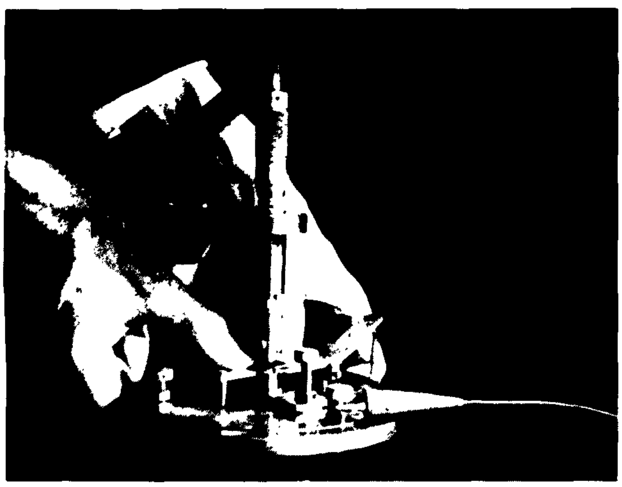

(b) Dynamic Calibration.

FIGURE 17. STRAIN GAGE CALIBRATOR.

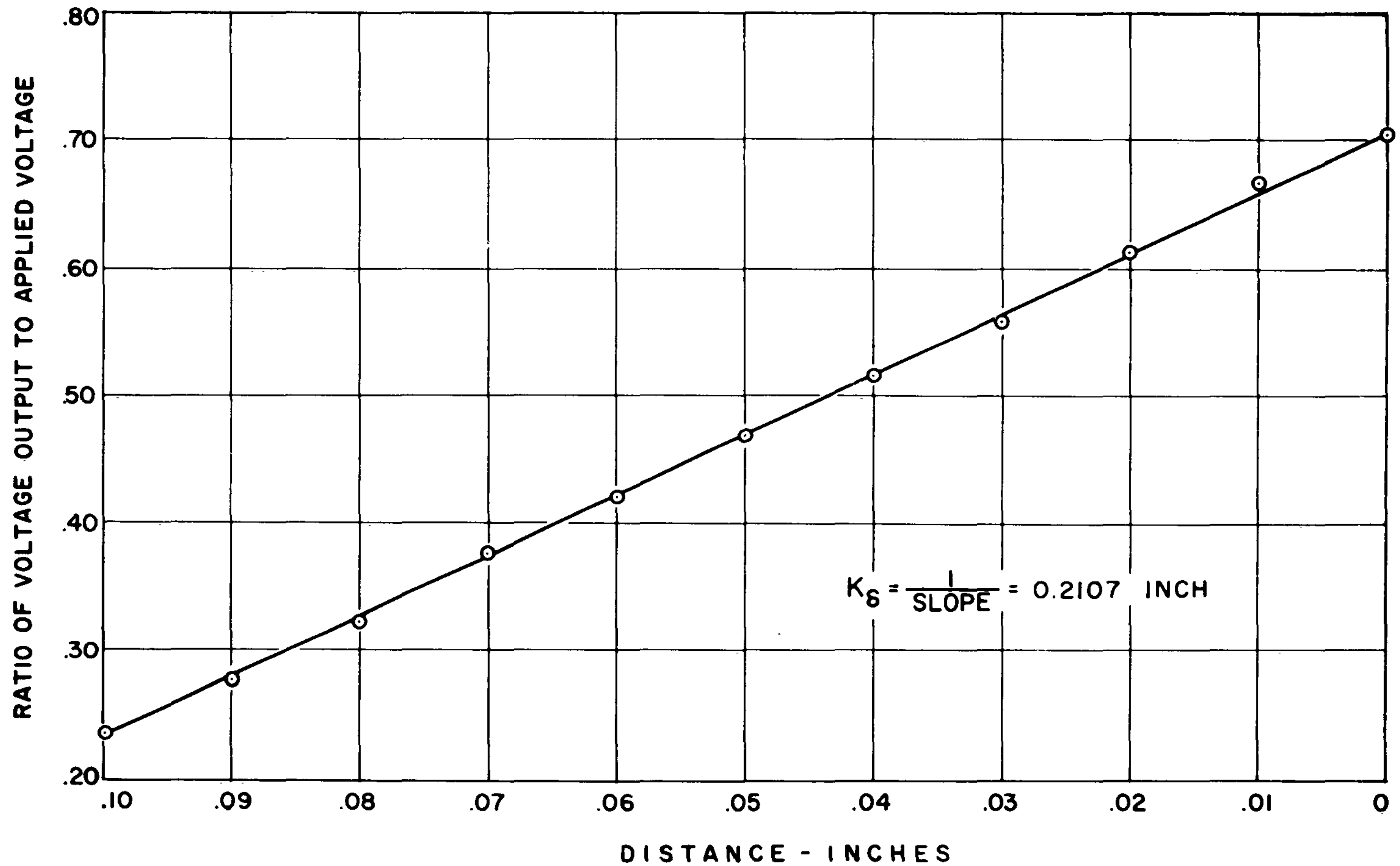

FIGURE 18. STATIC CALIBRATION OF STRAIN GAGE.

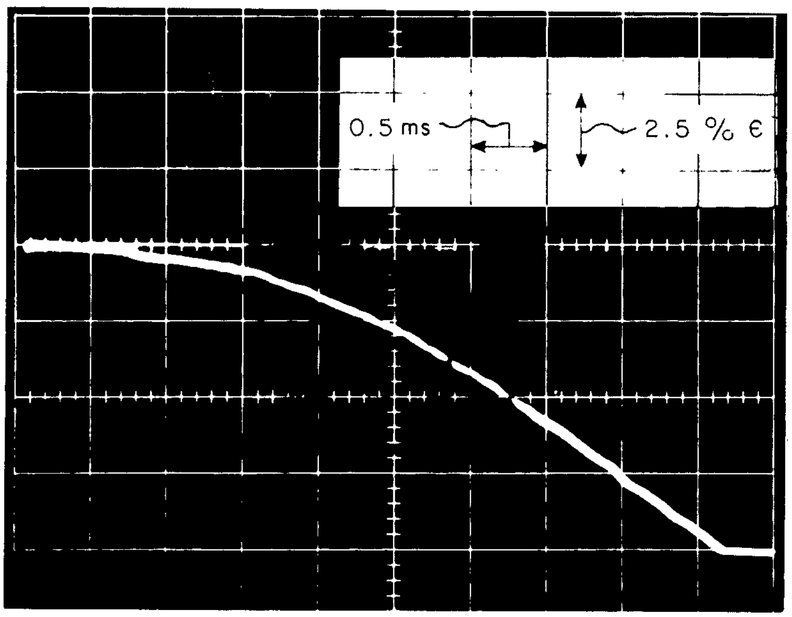

FIGURE 19. DYNAMIC RESPONSE OF STRAIN GAGE.

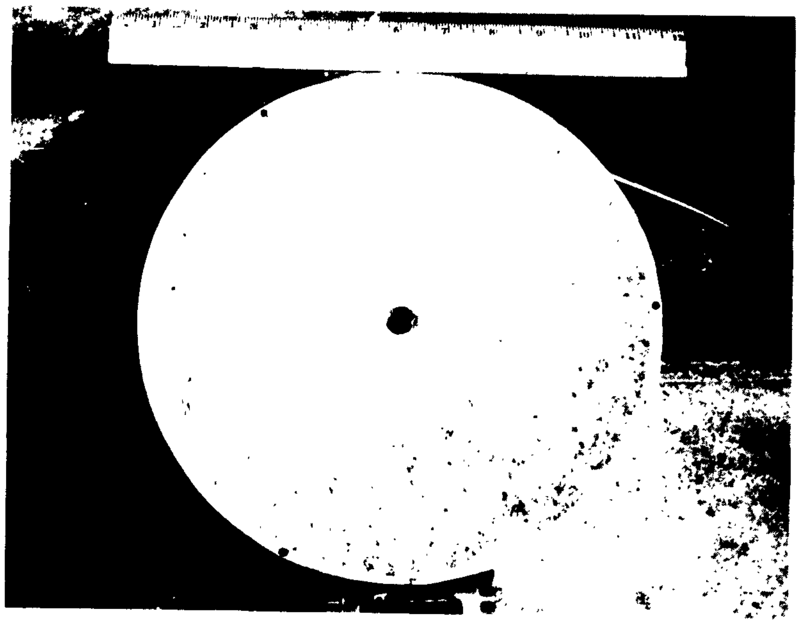

FIGURE 20. TEST CYLINDER OF COMPACTED CLAY WITH DRILLED HOLE THROUGH AXIS.

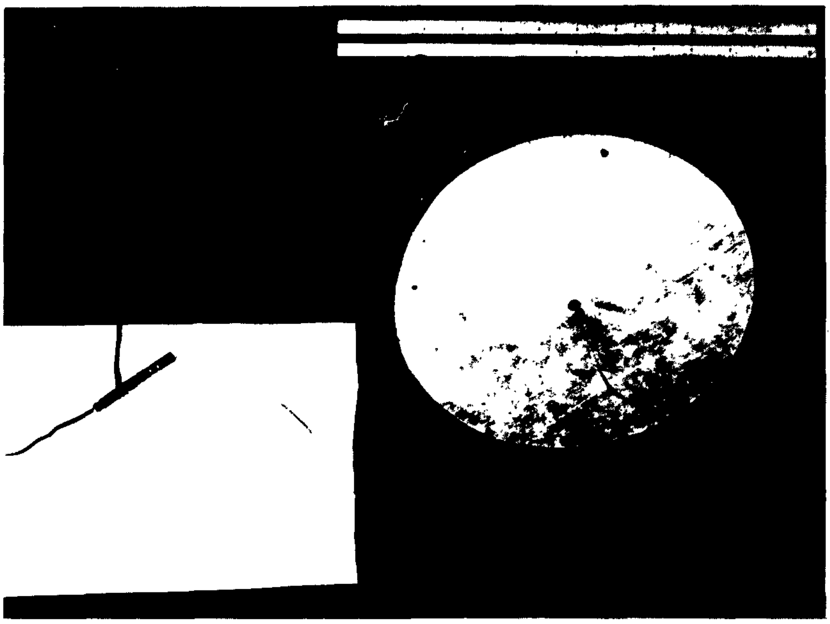

FIGURE 21. TEST CYLINDER WITH CHARGE, FUSE CORD, AND BLASTING CAP CONNECTED READY FOR TEST.

FIGURE 22. VIEW OF TEST CYLINDER AND BLAST CHAMBER.

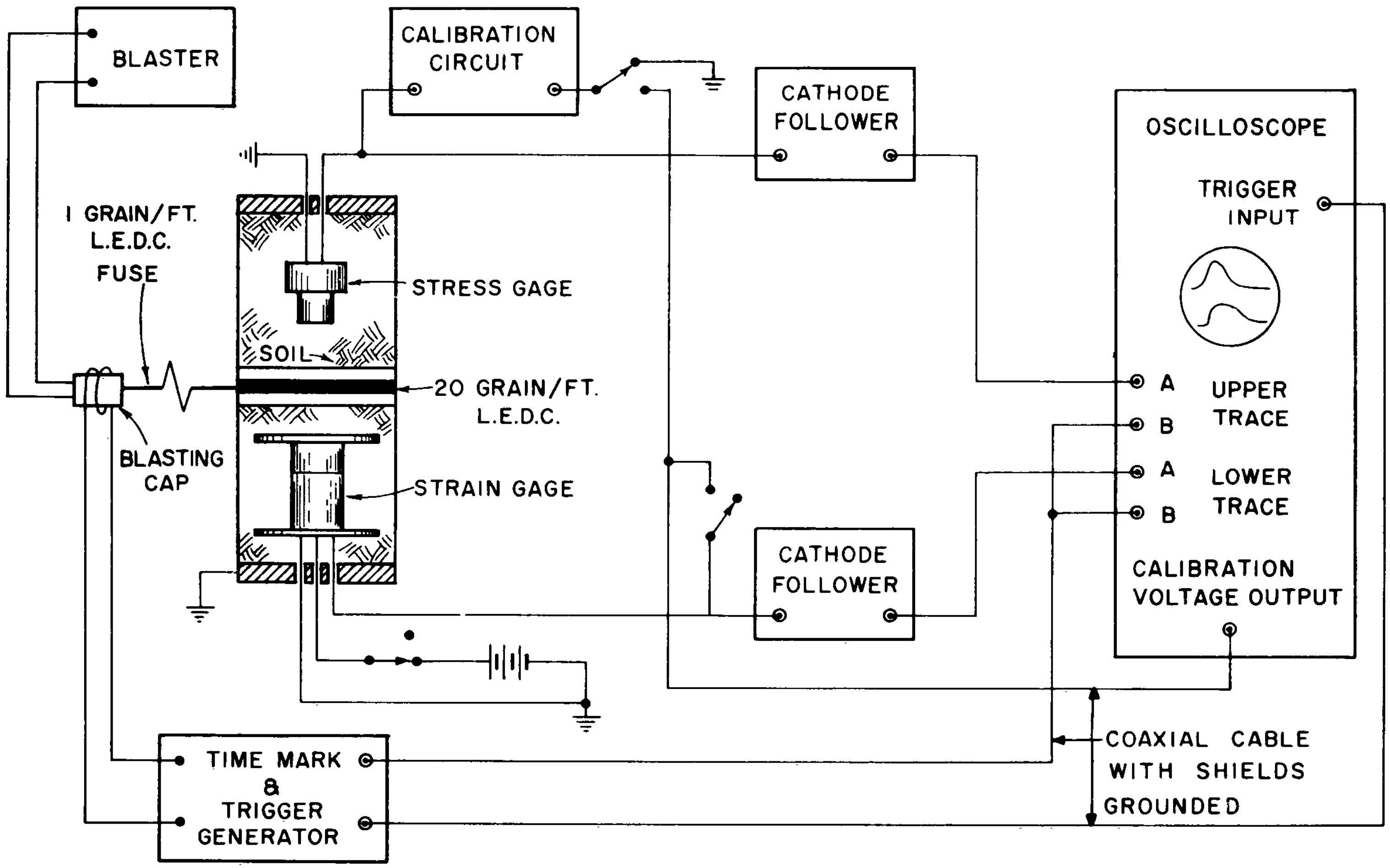

FIGURE 23. BLOCK DIAGRAM OF TEST ARRANGEMENT.

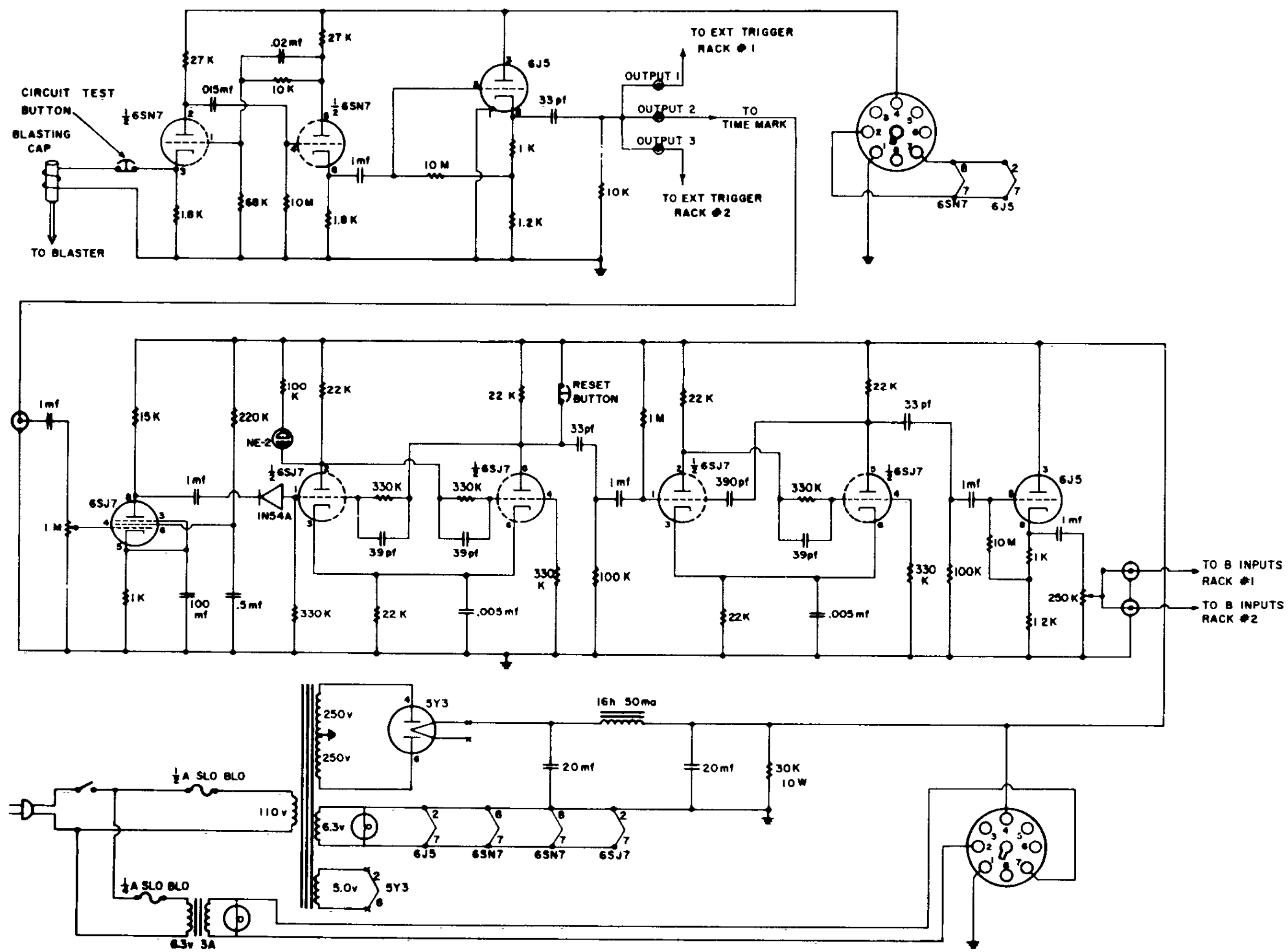

FIGURE 24. TIME MARK AND TRIGGER GENERATOR CIRCUITS

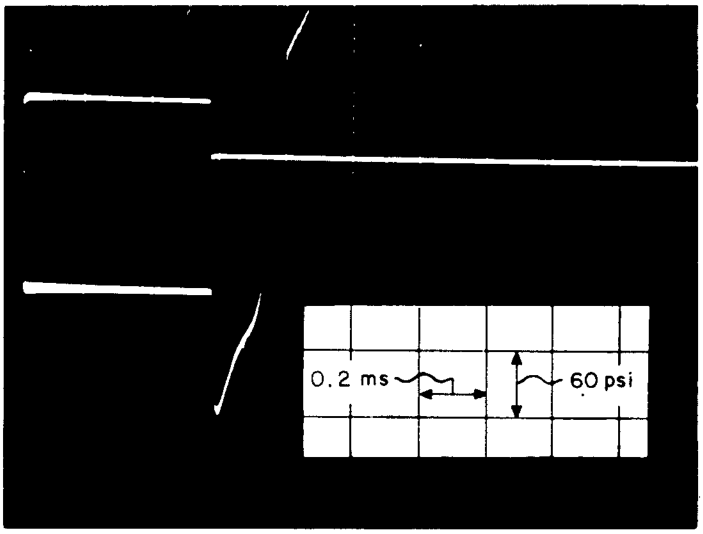

Upper Trace = Blasting Cap Current.
Lower Trace = Stress Gage.

FIGURE 25 STRESS GAGE RECORD - LEADS INCOMPLETELY SHIELDED.

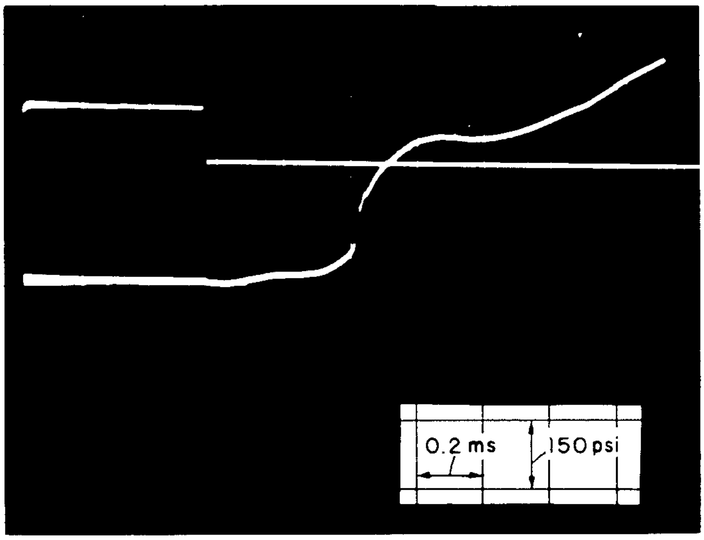

Upper Trace = Blasting Cap Current.
Lower Trace = Stress Gage.

FIGURE 26 STRESS GAGE RECORD - LEADS INCOMPLETELY SHIELDED.

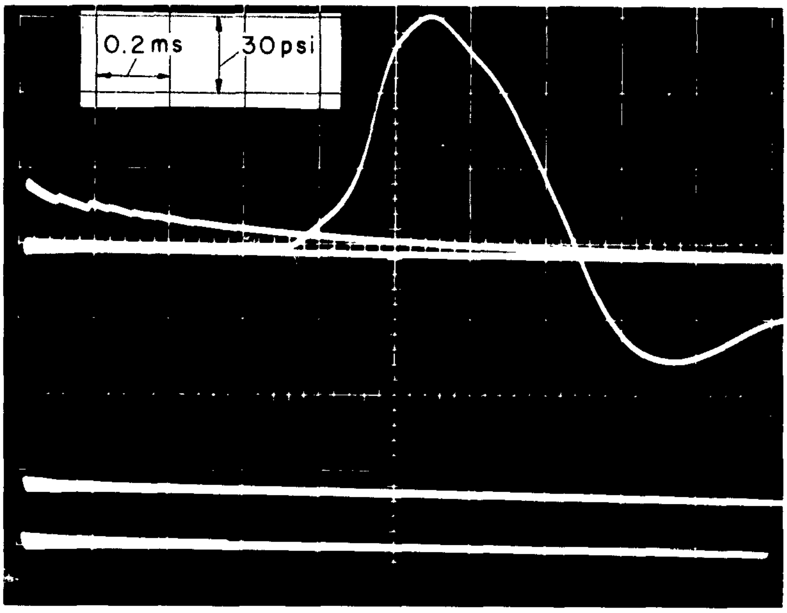

Upper Trace = Stress gage near wall of sample.
Lower Trace = Typical decay of calibration signal.

Both calibration pulses represent 1.35 volts applied to calibration circuit.

FIGURE 27. STRESS GAGE RECORD - LEAD CONNECTIONS NOT MOISTURE PROOF.

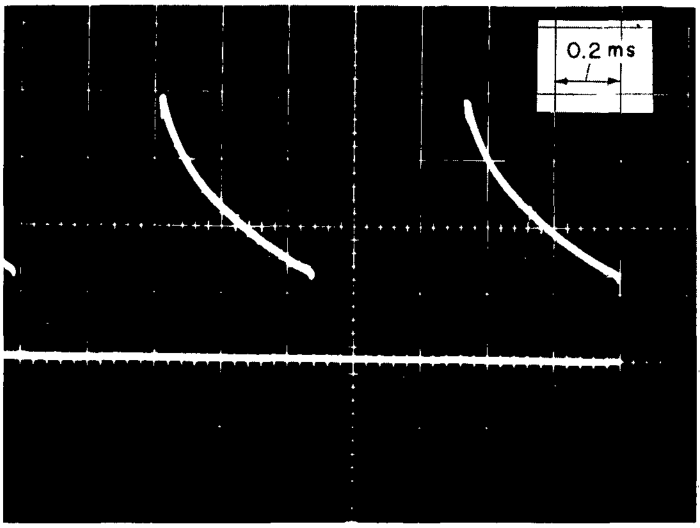

(a) Gage and Leads Connected. (Not Moisture Proofed)

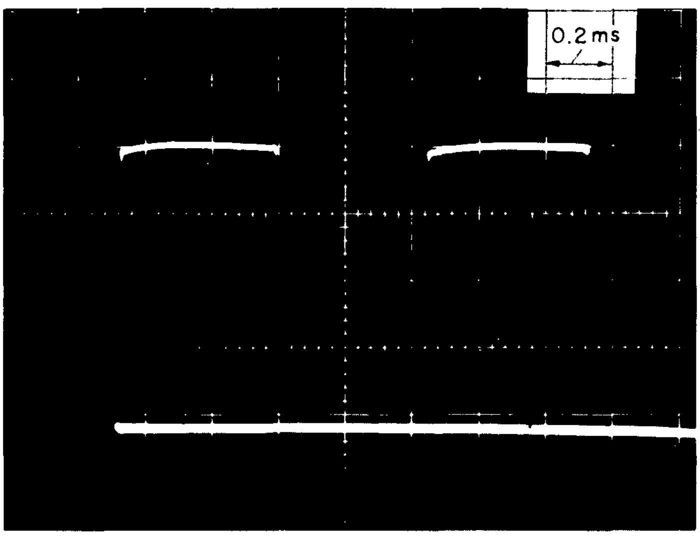

(b) Gage and Leads Disconnected.

FIGURE 28. OUTPUT OF CATHODE FOLLOWERS WITH SQUARE WAVE APPLIED TO CALIBRATION CIRCUIT.

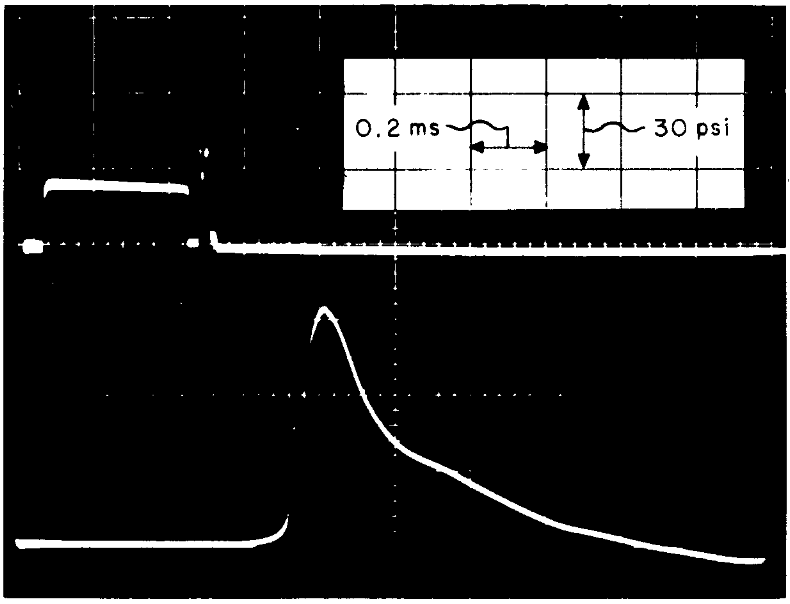

Upper Trace = Blasting Cap Current.
Lower Trace = Stress Gage.

FIGURE 29. STRESS GAGE RECORD - LEADS COMPLETELY SHIELDED AND MOISTURE PROOF

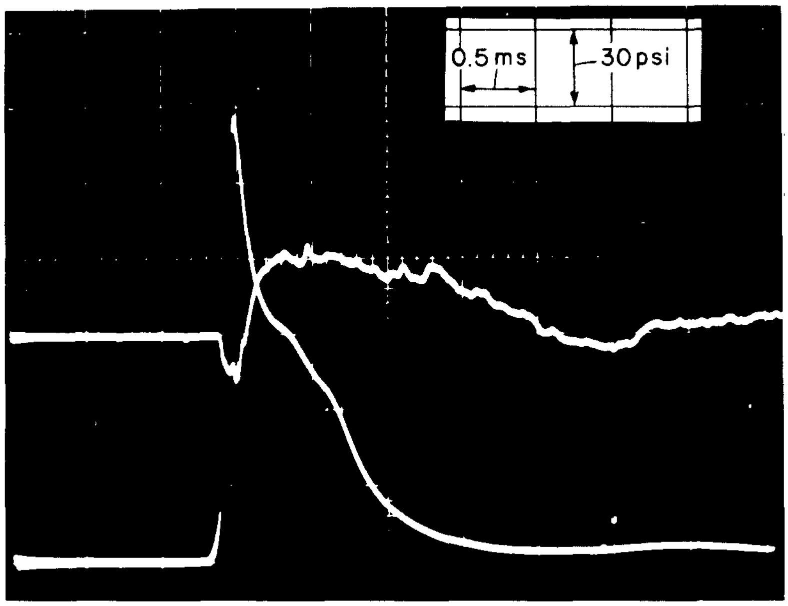

Upper Trace = Strain Gage (deposited carbon resistance element).

Lower Trace = Stress Gage.

FIGURE 30. STRESS - STRAIN RECORD.

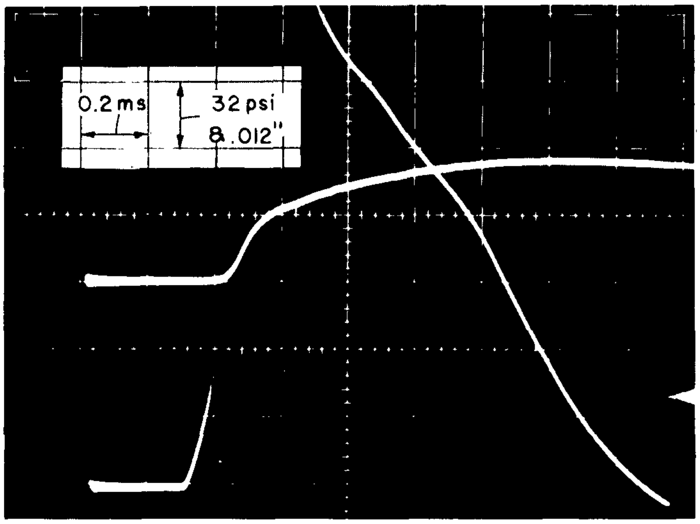

(a) First Shot.

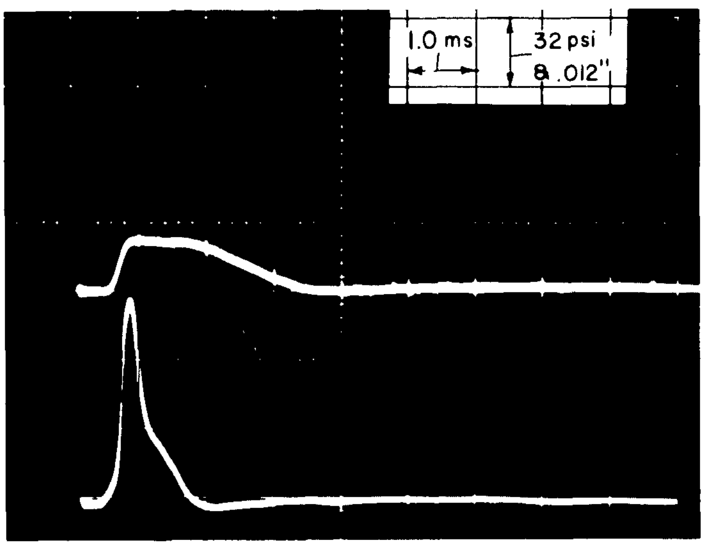

(b) Second Shot.

FIGURE 31. STRESS-STRAIN RECORD.

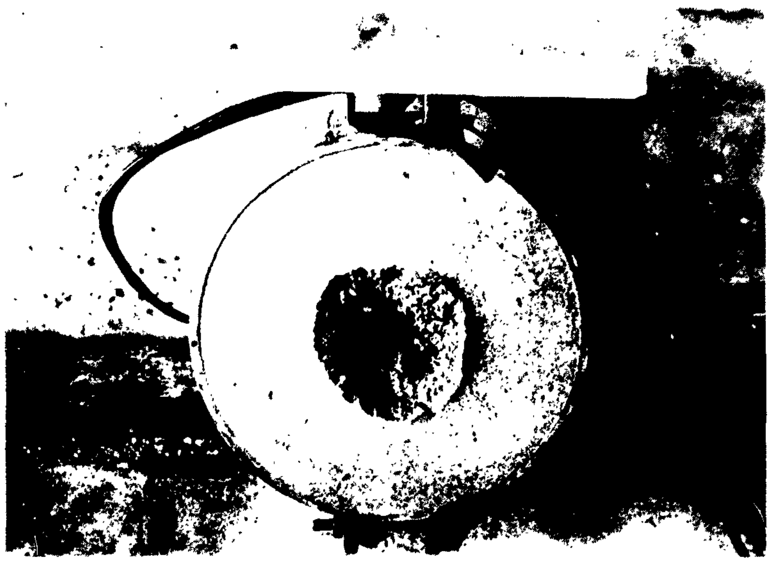

FIGURE 32. VIEW OF SAMPLE AFTER FIRST SHOT.
(COMPARE WITH FIGURE 20.)

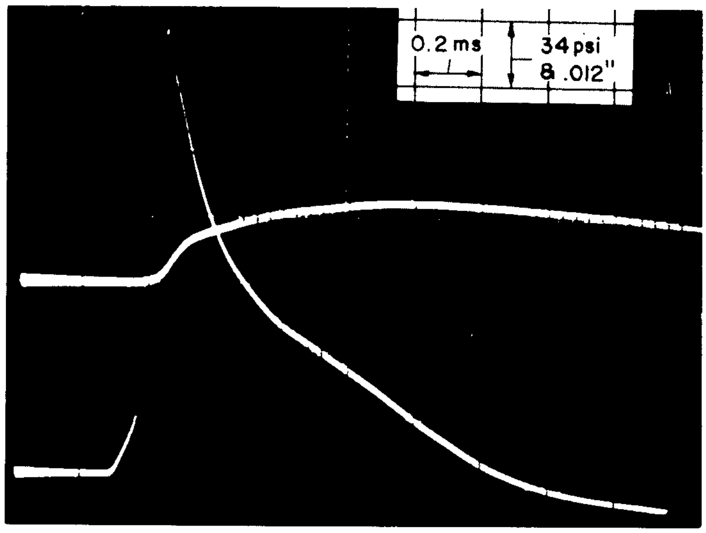

(a) First Shot.

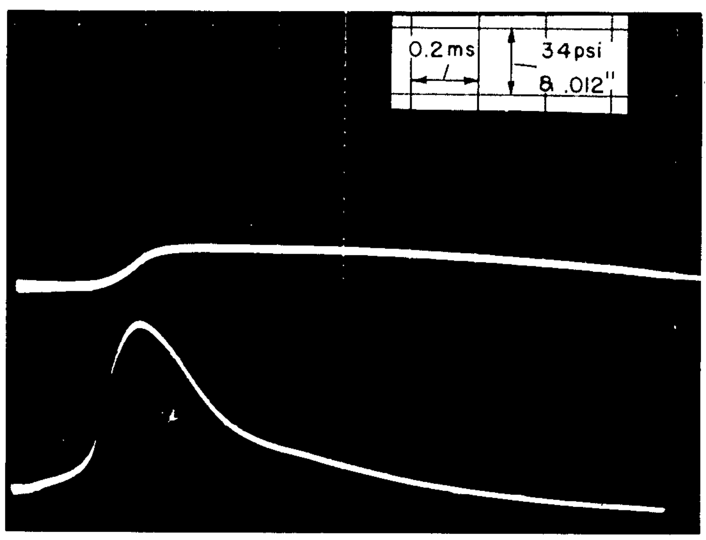

(b) Second Shot.

FIGURE 33. STRESS-STRAIN RECORD.

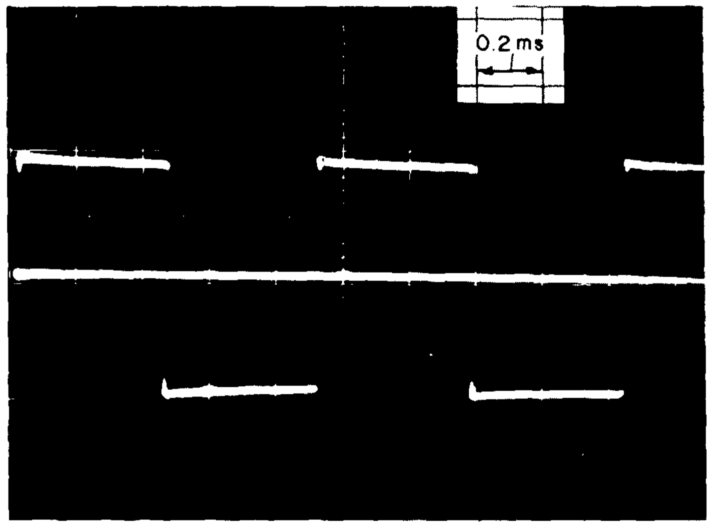

(a) Stress Gage.

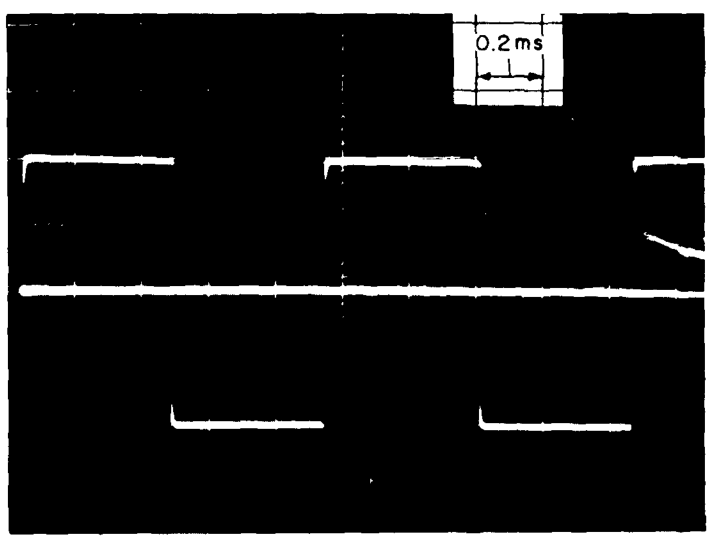

(b) Strain Gage

FIGURE 34. CALIBRATION PULSES FOR STRESS AND STRAIN GAGES (FOR THE RECORDS SHOWN IN FIGURE 33).

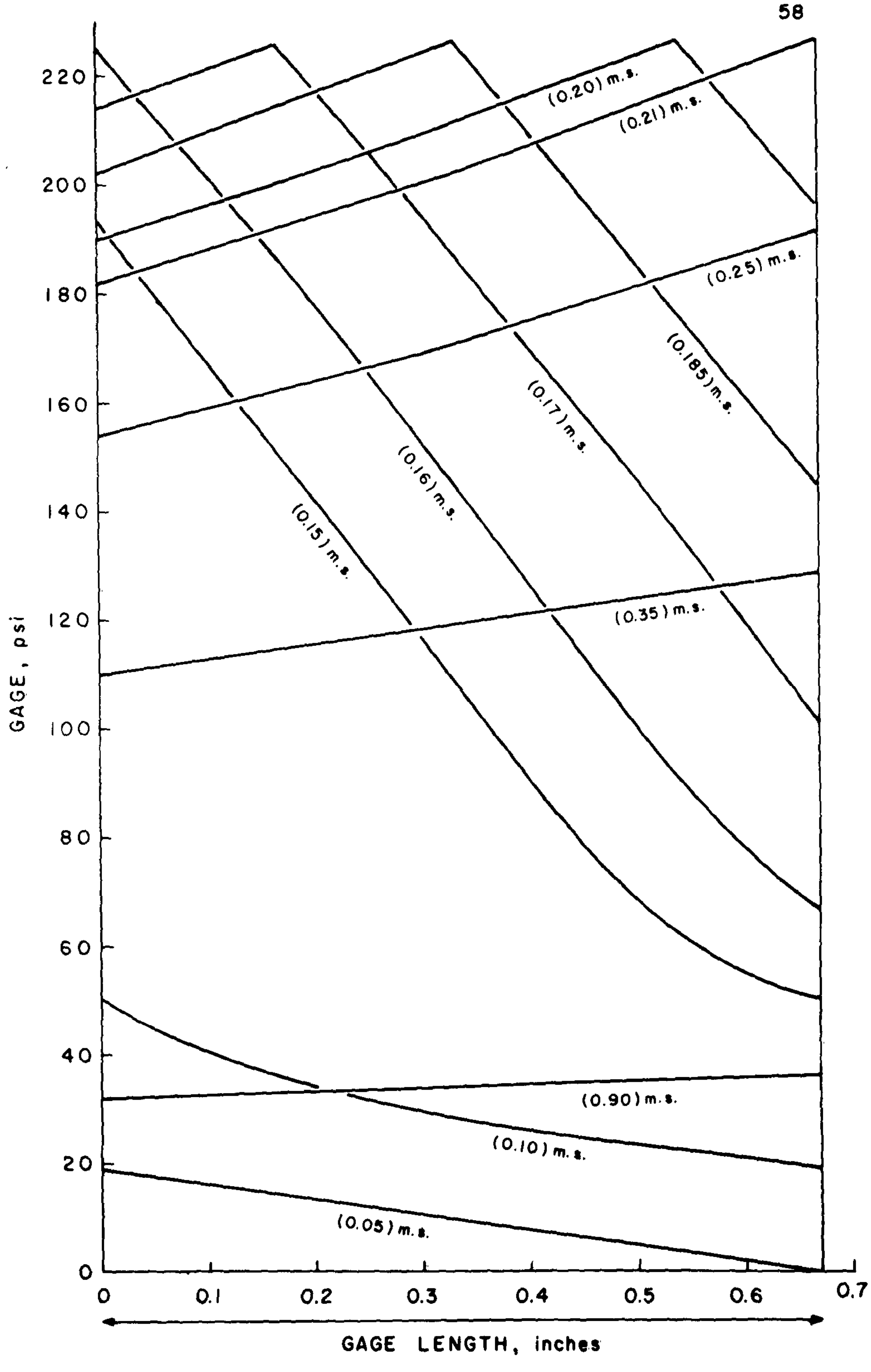

FIGURE 35. STRESS DISTRIBUTION ACROSS STRAIN GAGE Vs. TIME

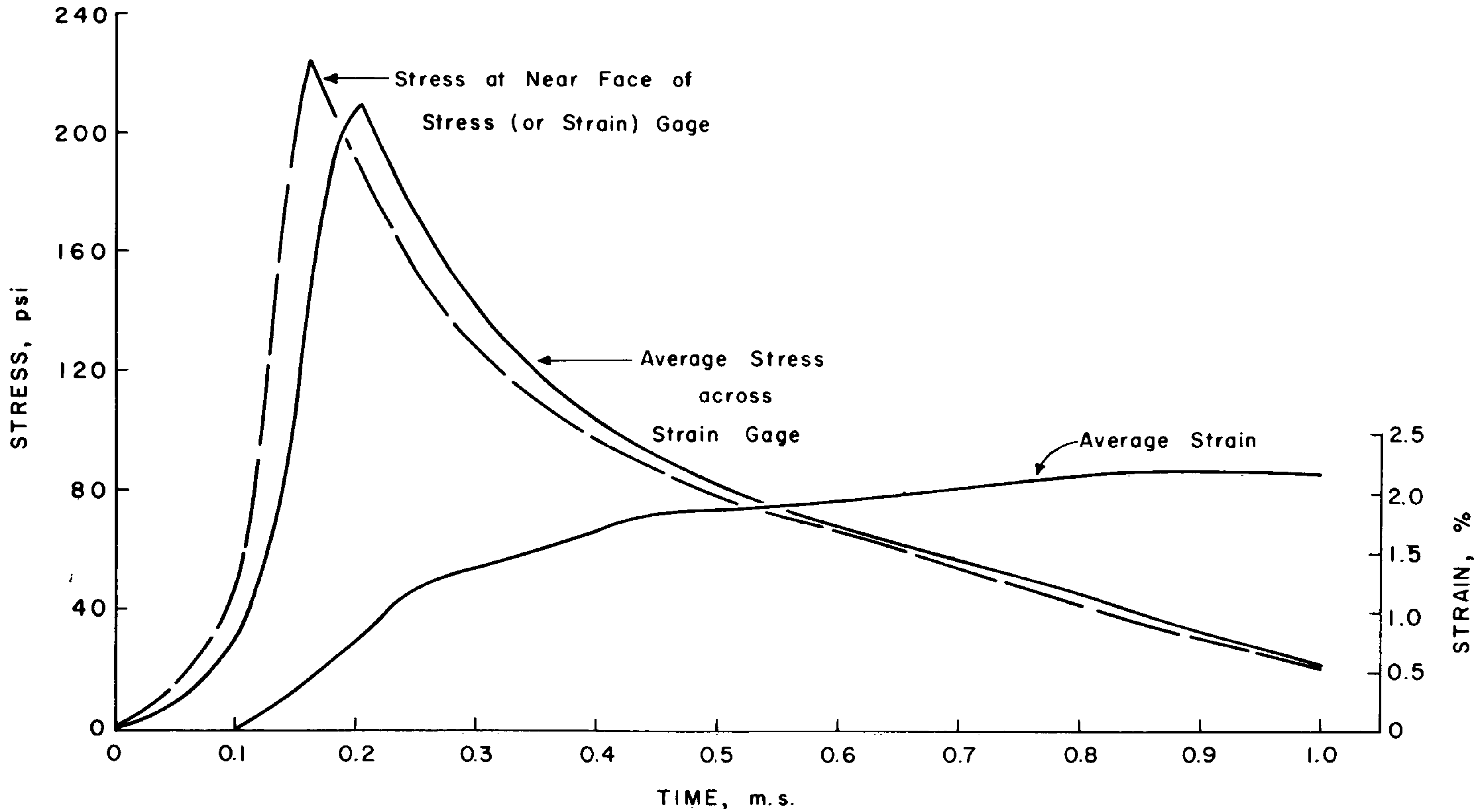

FIGURE 36. AVERAGE STRESS AND AVERAGE STRAIN Vs. TIME

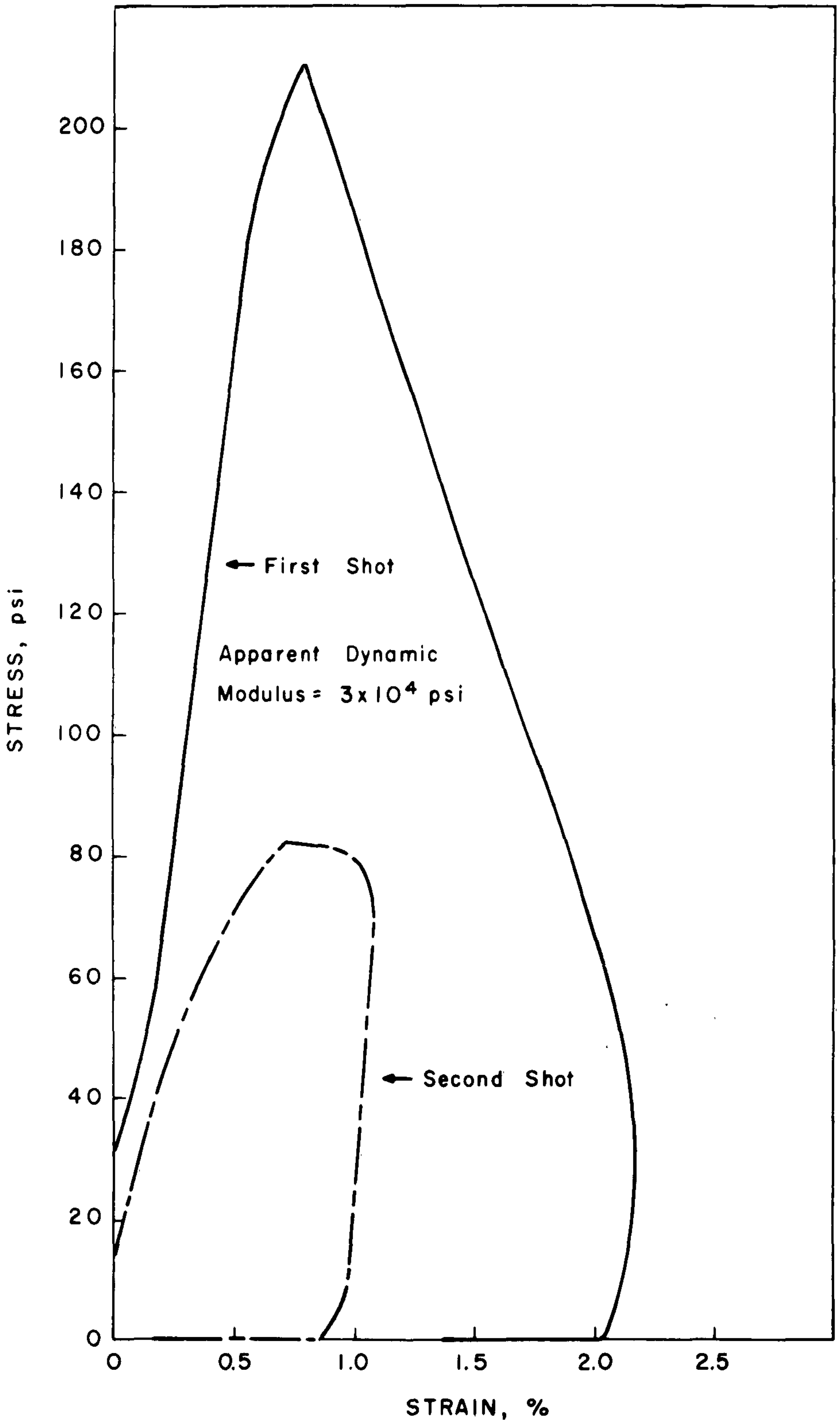

FIGURE 37. AVERAGE STRESS Vs. AVERAGE STRAIN RELATIONSHIP

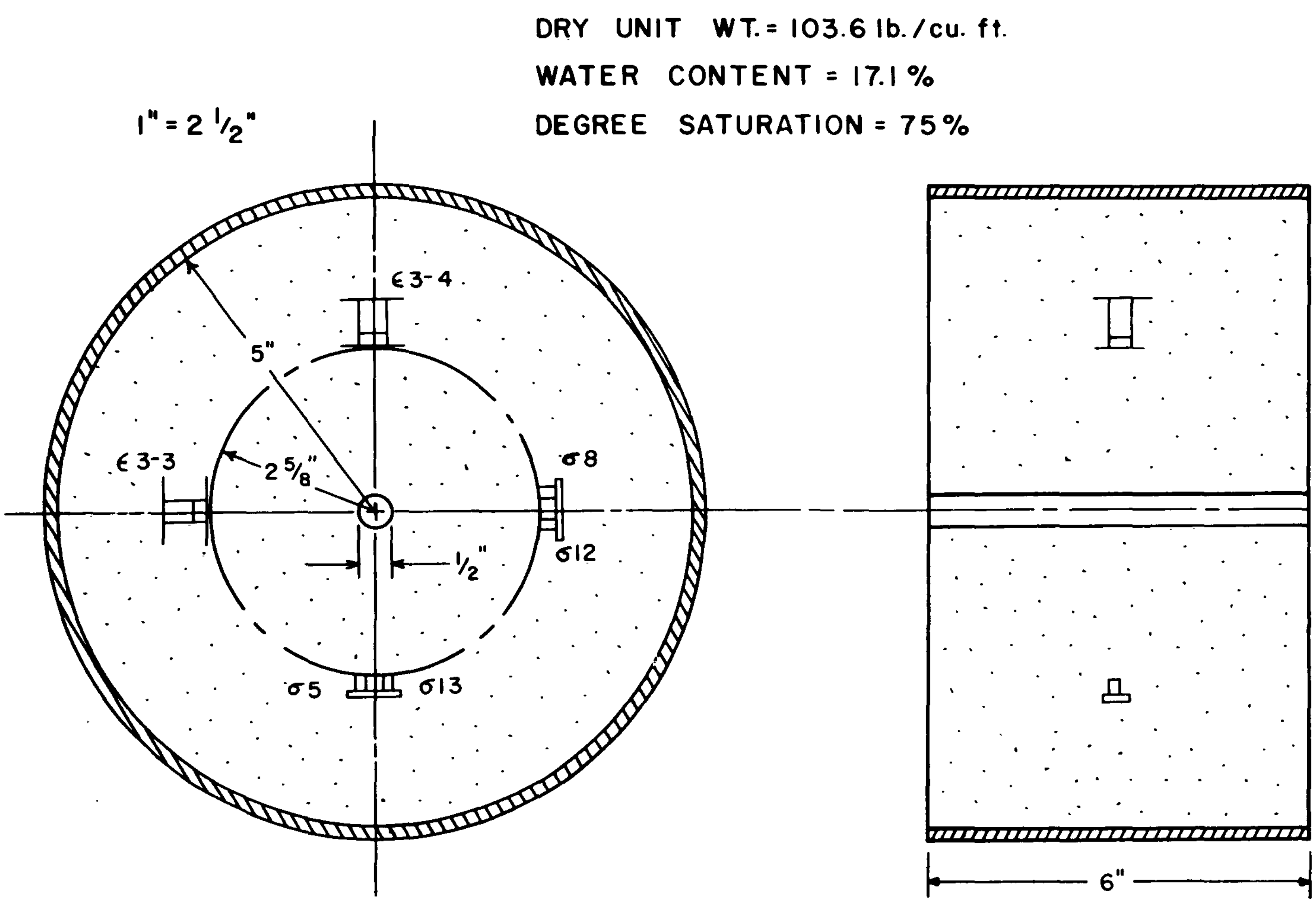

FIGURE 38. TEST SET-UP TO EVALUATE REPRODUCIBILITY OF GAGE RESPONSES

APPENDIX

Construction and Assembly of Dynamic Strain Gage

The housing and lower flange, and the upper flange (Figure A1), the plunger and the guide pin (Figure A2) are constructed from stainless steel. The housing and plunger are carefully machined as a pair to provide a light slip fit. The clamp (Figure A2) is machined from brass to facilitate soldering.

The wiper blank (Figure A3) is fabricated from spring brass. Two pieces of 1/64 inch diameter silver wire approximately 1/4 inch long are cut and each is bent into a tight U. These U's are inserted into the two holes at each side of the wiper blank and soldered in place with the round tips of the U's projecting inward 1/32 inch. Excess solder and wire projecting on the outside of the blank are filed off. The silver contacts are checked for smoothness, symmetry, and perpendicularity with the arms of the wiper blank. The assembly is then cleaned with acetone.

Three pieces of 30-gage stranded lead wire are cut in 12-inch lengths and 1/2 inch of insulation is stripped from the ends. One of the leads is inserted into the small hole in half of the clamp and soldered in place, with excess wire and solder being filed off; this operation is repeated with the other half of the clamp.

The Markite resistance element is shown in Figure A3. It is prismatic in shape with a Markite resistive surface molded on one face and a low resistance surface on the opposite parallel face. The clamp with the leads projecting from the bottom is fitted over the Markite element with the bottom of the element flush with the bottom of the clamp. The assembly is inserted into the hole in the Bakelite base (Figure A3) with the top of the clamp flush with the top of the base and the element perpendicular to the base. After checking (with an ohmmeter) that the clamps are in electrical contact with the Markite element, a drop

of Epoxy 220 is placed over the top of the slots in the clamp and allowed to cure. The top of the Markite element is then filed until it extends 11/64 inches above the top of the Bakelite base. A notch is then filed in the top of the element parallel to the resistive-conductive faces.

A small drop of Epoxy is placed in the hole at the bottom of the Markite element, a stripped end of the third lead is painted with Epoxy and inserted through the bottom hole of the Markite, pulled through until snugly in place, and then crimped down over the notch at the top of the element. Epoxy is placed over the notch and allowed to cure. Excess Epoxy and a small part of the stripped lead is then filed off so that the element is again 11/64 inches long and the lead is exposed for electrical contact. Silver conducting paint is applied to the top of the element to connect the center lead with the resistance face of the Markite element.

The top of the wiper blank is coated with Epoxy and centered in the scored markings on the insulating disk (Figure A3). The wiper is held in place with a thin strip of tape while the Epoxy cures. The insulating disk and wiper assembly is then bonded to the inside of the plunger with Epoxy so that the line between the two silver contacts is perpendicular to the guide-pin slot.

The plastic foam seal is bonded to the top of the housing with Epoxy and allowed to cure. The wiper-plunger assembly is then placed over the Markite resistance element - Bakelite base assembly by pulling the wiper onto the element from the side to avoid chipping the silver conducting paint. The entire assembly is inserted through the hole in the bottom of the housing, engaging the guide pin in the slot of the plunger, until the Bakelite base is flush with the bottom of the lower flange. The upper flange is then screwed onto the shaft of the plunger

and tightened, keeping the plunger from twisting with a small screwdriver to avoid tightening the upper flange against the guide-pin on the plunger.

The gage output is then connected to an ohmmeter, the plunger moved up and down, and the variation in resistance observed. This variation should be smooth and continuous over the full range of movement. If it is not, the Bakelite base can be shifted slightly. If the difficulty is still not corrected, the gage must be disassembled and all parts checked. When smooth and continuous resistance variation is achieved, the Bakelite base is bonded to the lower flange with Epoxy and the leads are potted. The foam seal is then depressed, the top coated with Epoxy and then released to bond with the bottom of the upper flange.

The leads are then cut to the desired length, soldered to low-noise co-axial cable, and the soldered connections potted with Epoxy and wrapped in Teflon tape to make them moisture proof. Two co-axial cables are used. The center lead of the gage is common to both cables and is connected to their respective shields.

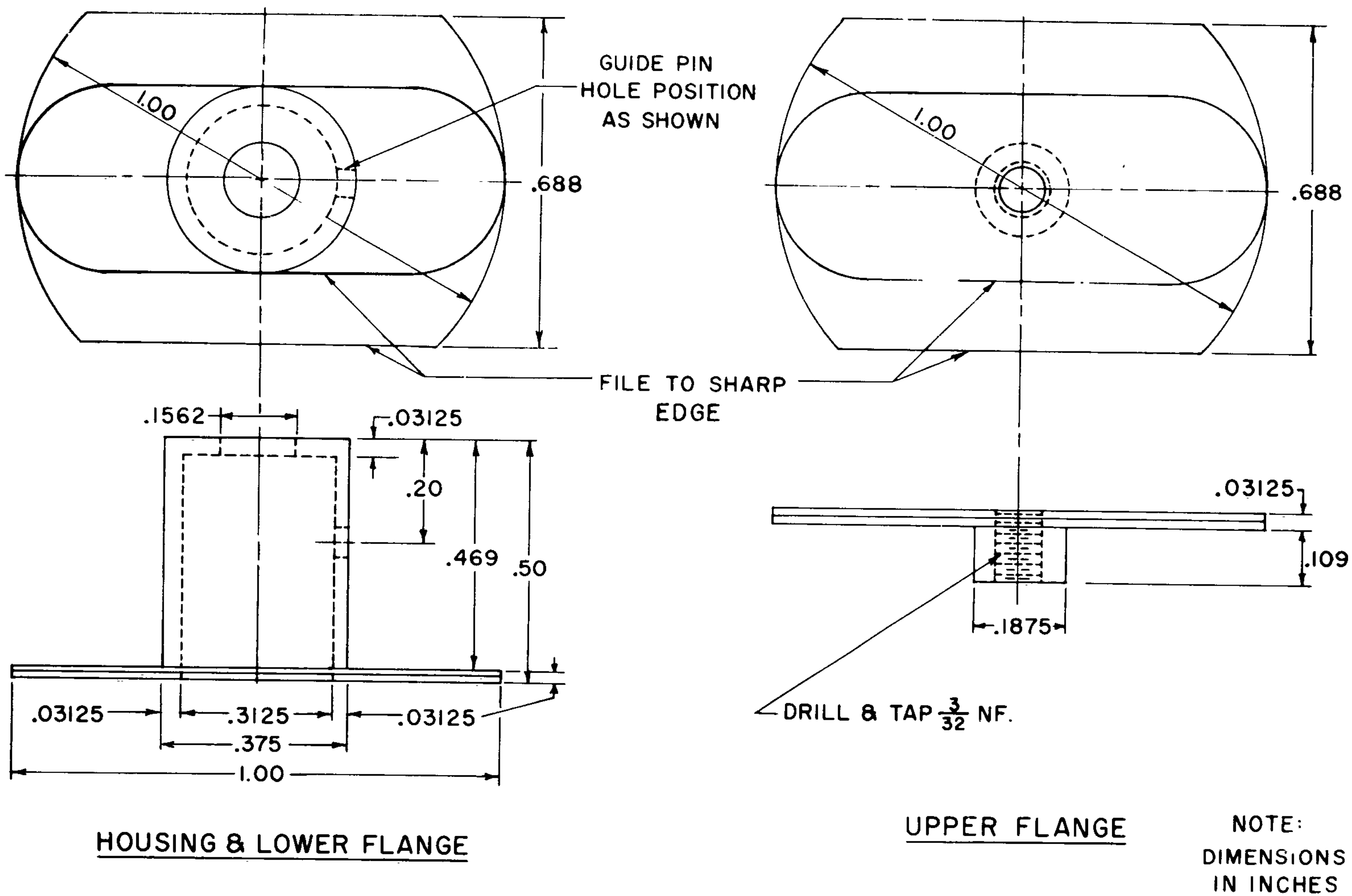

FIGURE A1. STRAIN GAGE PARTS.

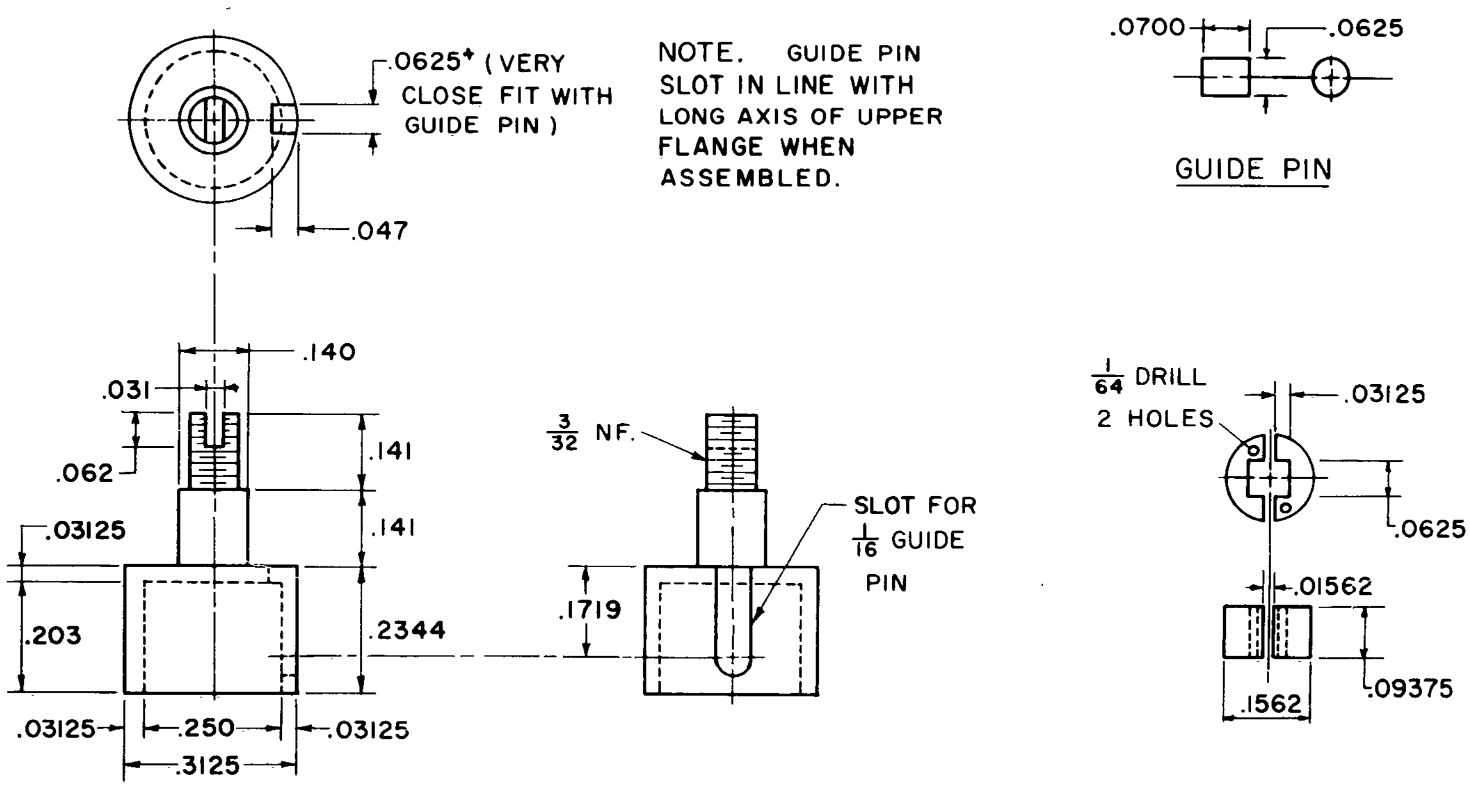

NOTE:
DIMENSIONS
IN INCHES

FIGURE A2. STRAIN GAGE PARTS.

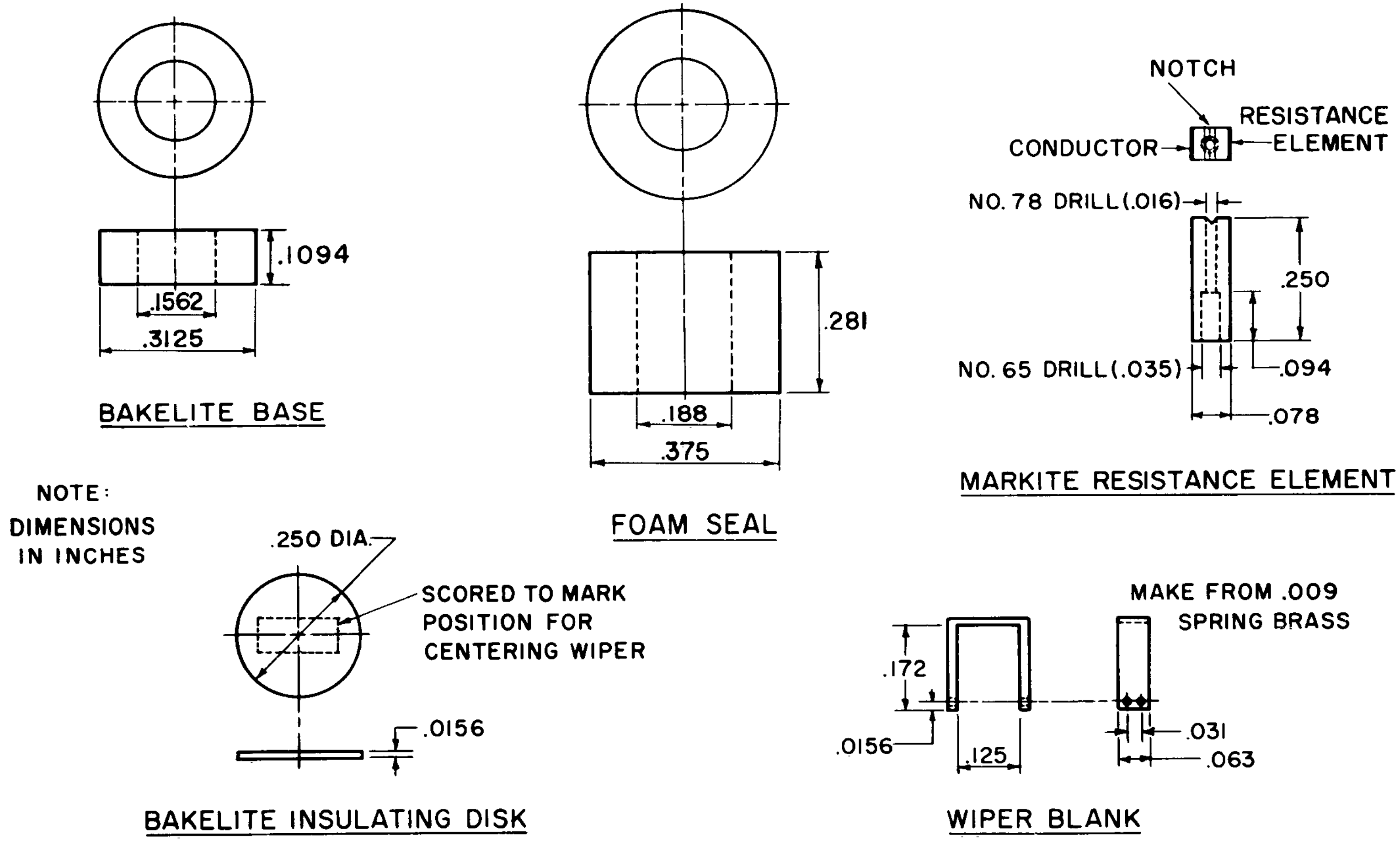

FIGURE A3. STRAIN GAGE PARTS.

DISTRIBUTION

No. Cys	
	HEADQUARTERS USAF
2	Hq USAF (AFOCE), Wash 25, DC
1	Hq USAF (AFRDC-NE), Wash 25, DC
1	Hq USAF (AFCIN), Wash 25, DC
1	USAF Dep IG for Insp (AFCDI-B-3), Norton AFB, Calif
1	USAF Dep IG for Safety (AFINS), Kirtland AFB, NM
2	AFOAR, Bldg T-D, Wash 25, DC
1	AFCRL, Hanscom Fld, Bedford, Mass
	MAJOR AIR COMMANDS
1	AFSC (SCT), Andrews AFB, Wash 25, DC
1	AUL, Maxwell AFB, Ala
1	USAFIT, Wright-Patterson AFB, Ohio
	AFSC ORGANIZATIONS
1	AFSC Regional Office, 6331 Hollywood Blvd., Los Angeles 28, Calif
1	ASD (ASAPRL, Technical Doc Library), Wright-Patterson AFB, Ohio
1	BSD (BSR), AF Unit Post Office, Los Angeles 45, Calif
1	SSD, AF Unit Post Office, Los Angeles 45, Calif
1	ESD (ESAT), Hanscom Fld, Bedford, Mass
1	RADC (Document Library), Griffiss AFB, NY
	KIRTLAND AFB ORGANIZATIONS
	AFSWC, Kirtland AFB, NM
1	(SWEH)
35	(SWOI)
1	(SWR)
3	(SWRS)
	OTHER AIR FORCE AGENCIES
1	Director, USAF Project RAND, via: Air Force Liaison Office, The RAND Corporation, (RAND Library), 1700 Main Street, Santa Monica, Calif

DISTRIBUTION (cont'd)

No. Cys	
	ARMY ACTIVITIES
1	Chief of Research and Development, Department of the Army, (Special Weapons and Air Defense Division), Wash 25, DC
2	Director, Ballistic Research Laboratories (Library), Aberdeen Proving Ground, Md
1	Commanding Officer, US Army Engineers, Research & Development Laboratories, Ft. Belvoir, Va
1	Chief of Engineers, Department of the Army (ENGEB), Wash 25, DC
1	Office of the Chief, Corps of Engineers, US Army (Protective Construction Branch), Wash 25, DC
2	Director, US Army Waterways Experiment Sta (WESRL), P. O. Box 60, Vicksburg, Miss
	NAVY ACTIVITIES
1	Chief of Naval Research, Wash 25, DC
1	Chief, Bureau of Yards and Docks, Department of the Navy, Wash 25, DC
2	Commanding Officer and Director, Naval Civil Engineering Laboratory, Port Hueneme, Calif
1	Commander, Naval Ordnance Test Station, Inyokern (Code 12), China Lake, Calif
1	Commander, Naval Ordnance Laboratory, White Oak, Silver Spring, Md
1	Officer-in-Charge, Civil Engineering Corps Officers, US Naval School, Naval Construction Battalion Center, Port Hueneme, Calif
	OTHER DOD ACTIVITIES
2	Chief, Defense Atomic Support Agency (Document Library), Wash 25, DC
1	Commander, Field Command, Defense Atomic Support Agency, (FCAG3, Special Weapons Publication Distribution), Sandia Base, NM
1	Director, Defense Research & Engineering, The Pentagon, Wash 25, DC
10	ASTIA (TIPDR), Arlington Hall Sta, Arlington 12, Va
	AEC ACTIVITIES
1	Sandia Corporation (Tech Library), Sandia Base, NM

DISTRIBUTION (cont'd)

No. Cys	
	OTHER
	Armour Research Foundation, Illinois Institute of Technology, 3422 South Dearborn St., Chicago 15, Ill
2	(Dr. Eben Vey)
1	(Dr. T. H. Schiffman)
1	American Machine & Foundry Co., Mechanics Research Division, (T. G. Morrison), 7501 North Natchez Avenue, Niles, Ill
2	University of New Mexico, (Dr. Eugene Zwoyer), University Hill, NE, Albuquerque, NM
2	Massachusetts Institute of Technology, Department of Civil and Sanitary Engineering, (Dr. Robert V. Whitman), 77 Massachusetts Ave., Cambridge 39, Mass
2	University of Notre Dame, Department of Civil Engineering, (Dr. Harry Saxe), Notre Dame, Ind
12	Purdue University, Civil Engineering Dept., (Prof G. A. Leonards), Lafayette, Ind
1	United Research Services, (Kenneth Kaplan), 1811 Trousdale Dr., Burlingame, Calif
2	South Dakota School of Mines & Technology, (Edwin H. Oshier), Rapid City, S. Dak
1	Paul Weidlinger, 770 Lexington Ave., New York 21, NY
1	Shannon & Wilson, Soil Mechanics & Foundation Engineers, (Mr. Stanley Wilson), 1105 No. 38th St., Seattle 3, Wash
1	United Electrodynamics, Inc., (Mr. Ted Winston), 200 Allendale Rd., Pasadena, Calif
1	Stanford Research Institute, (F. M. Sauer), 333 Ravens Wood, Menlo Park, Calif
1	Iowa State University, Department of Theoretical & Applied Mechanics, (Glen Murphy), Ames, Iowa
	University of Illinois, Department of Civil Engineering, 207 Talbot Laboratory, Urbana, Ill
2	(Dr. N. M. Newmark)
1	(S. H. Hendron)
1	St. Louis University, Institute of Technology, (Dr. Carl Kisslinger), 3621 Olive St., St. Louis 8, Mo
1	University of Florida, Department of Civil Engineering, (Frank E. Richardt), Gainesville, Fla
1	University of California, College of Engineering, (Prof. Martin Duke), Los Angeles, Calif

DISTRIBUTION (cont'd)

No. Cys	
1	Portland Cement Assoc., (Eivind Hognestad, Manager, Structural Dev Sec), 33 W. Grand Ave., Chicago, Ill
1	Stanford University, School of Mechanical Engineering, (Dr. Lydik S. Jacobsen), Stanford, Calif
1	University of Illinois, (Prof C. E. Bowman), 207 Talbot Laboratory, Urbana, Ill
1	The Dikewood Corporation, 4805 Menaul Blvd., NE, Albuquerque, NM
1	Ralph M. Parsons & Co., (M. S. Agbabian), 617 West Seventh St., Los Angeles 17, Calif
1	National Engineering Science Co., (Lars Skjelbreia), 711 South Fairoaks Ave., Pasadena, Calif
1	University of Washington, (Dr. I. M. Fyfe), Seattle 5, Wash
1	The University of Missouri, Department of Mining Engineering, School of Mines & Metallurgy, (Dr. George B. Clark), Rolla, Mo
1	Official Record Copy, (SWRS, Mr. Walsh)

Air Force Special Weapons Center, Kirtland AF Base, N.M.
Rpt. No. AFSWC-TDR-62-90. LABORATORY EXPERIMENTS ON THE RESPONSE OF SOILS TO SHOCK LOADINGS.
Jan 63. 78 p, incl illus, tables, 7 refs.
Unclassified Report

A report is made of research being carried out at Purdue University whose overall purpose is to develop, on the basis of direct measurements, mathematical models suitable for describing the propagation of a compression shock wave through soils--principally through partly saturated clays. This interim report deals with the selection of a suitable type of laboratory test and with the design, calibration, and use of gages to measure stress and strain in the vicinity of a point during the propagation of a shock wave. Preliminary results from tests on samples of compacted clay are also included.

1. Blast loading
2. Gages
3. Shock waves
4. Soils--effects of blast
5. Stress and strain

I. AFSC Project 1080, Task 108001
II. Contract AF 29(601)-2830
III. Purdue Univ., Lafayette Ind., School of Civil Engineering
IV. G. A. Leonards
V. DASA WEB No. 13.004
VI. In ASTIA collection

Air Force Special Weapons Center, Kirtland AF Base, N.M.
Rpt. No. AFSWC-TDR-62-90. LABORATORY EXPERIMENTS ON THE RESPONSE OF SOILS TO SHOCK LOADINGS.
Jan 63. 78 p, incl illus, tables, 7 refs.
Unclassified Report

A report is made of research being carried out at Purdue University whose overall purpose is to develop, on the basis of direct measurements, mathematical models suitable for describing the propagation of a compression shock wave through soils--principally through partly saturated clays. This interim report deals with the selection of a suitable type of laboratory test and with the design, calibration, and use of gages to measure stress and strain in the vicinity of a point during the propagation of a shock wave. Preliminary results from tests on samples of compacted clay are also included.

1. Blast loading
2. Gages
3. Shock waves
4. Soils--effects of blast
5. Stress and strain

I. AFSC Project 1080, Task 108001
II. Contract AF 29(601)-2830
III. Purdue Univ., Lafayette Ind., School of Civil Engineering
IV. G. A. Leonards
V. DASA WEB No. 13.004
VI. In ASTIA collection

Air Force Special Weapons Center, Kirtland AF Base, N.M.
Rpt. No. AFSWC-TDR-62-90. LABORATORY EXPERIMENTS ON THE RESPONSE OF SOILS TO SHOCK LOADINGS.
Jan 63. 78 p, incl illus, tables, 7 refs.
Unclassified Report

A report is made of research being carried out at Purdue University whose overall purpose is to develop, on the basis of direct measurements, mathematical models suitable for describing the propagation of a compression shock wave through soils--principally through partly saturated clays. This interim report deals with the selection of a suitable type of laboratory test and with the design, calibration, and use of gages to measure stress and strain in the vicinity of a point during the propagation of a shock wave. Preliminary results from tests on samples of compacted clay are also included.

1. Blast loading
2. Gages
3. Shock waves
4. Soils--effects of blast
5. Stress and strain

I. AFSC Project 1080, Task 108001
II. Contract AF 29(601)-2830
III. Purdue Univ., Lafayette Ind., School of Civil Engineering
IV. G. A. Leonards
V. DASA WEB No. 13.004
VI. In ASTIA collection

Air Force Special Weapons Center, Kirtland AF Base, N.M.
Rpt. No. AFSWC-TDR-62-90. LABORATORY EXPERIMENTS ON THE RESPONSE OF SOILS TO SHOCK LOADINGS.
Jan 63. 78 p, incl illus, tables, 7 refs.
Unclassified Report

A report is made of research being carried out at Purdue University whose overall purpose is to develop, on the basis of direct measurements, mathematical models suitable for describing the propagation of a compression shock wave through soils--principally through partly saturated clays. This interim report deals with the selection of a suitable type of laboratory test and with the design, calibration, and use of gages to measure stress and strain in the vicinity of a point during the propagation of a shock wave. Preliminary results from tests on samples of compacted clay are also included.

1. Blast loading
2. Gages
3. Shock waves
4. Soils--effects of blast
5. Stress and strain

I. AFSC Project 1080, Task 108001
II. Contract AF 29(601)-2830
III. Purdue Univ., Lafayette Ind., School of Civil Engineering
IV. G. A. Leonards
V. DASA WEB No. 13.004
VI. In ASTIA collection